Exploration of Off-Design Performance for Hybrid Electric Regional Aircraft

Bonnin, V.O.; Hoogreef, M.F.M.

DOI
10.2514/1.C037893

Publication date
2025

Document Version
Final published version

Published in
Journal of Aircraft

Exploration of Off-Design Performance for Hybrid Electric Regional Aircraft

Vincent O. Bonnin* and Maurice F. M. Hoogreef†
Delft University of Technology, 2629 HS Delft, The Netherlands

https://doi.org/10.2514/1.C037893

Most studies investigate hybrid electric aircraft by comparing their respective performance over their design mission. However, most missions flown are less demanding in terms of payload and/or range. Kerosene aircraft can adapt their fuel load, yet battery-equipped aircraft have to make the best of an already installed battery. This paper compares the performance of battery-equipped hybrid electric regional propeller aircraft (parallel, serial/parallel partial hybrid, or serial powertrain) over their entire payload-range envelope, relative to a kerosene aircraft designed according to the same specifications and performing the same off-design missions. The payload-range envelope is determined by intricate combinations of sizing limits of powertrain components in terms of power and energy. All hybrid electric aircraft are heavier than their kerosene counterparts and less energy efficient on their design mission. However, over a 600 km range, a 60% fuel saving can be achieved at lower payloads. Full-electric cruise may be possible for all payloads up to ~500 km for all architectures when a battery-supplied power ratio of 20% in cruise flight is selected for the design point. The results demonstrate the off-design sensitivity to 1) selection of the powertrain architecture, 2) selection of the design hybridization strategy, and 3) selection of the design mission.

Nomenclature

b	=	span, m
d	=	diameter, m
E	=	energy, J
l	=	length, m
M	=	mass, kg
MTOM	=	maximum takeoff mass, kg
OEM	=	operating empty mass, kg
N_1	=	number of primary propulsors
N_2	=	number of secondary propulsors
P	=	power, W
S	=	wing area, m^2
W_{TO}	=	takeoff weight, N
η_{EM}	=	electrical machine efficiency
η_{GB}	=	gearbox efficiency
η_{GT}	=	gas turbine efficiency
η_{PM}	=	power management module efficiency
φ	=	shaft power ratio
ϕ	=	battery-supplied power ratio
ξ	=	gas turbine throttle

Subscripts

bat	=	battery
EM1	=	primary chain electrical machine
EM2	=	secondary chain electrical machine
f	=	fuel
fus	=	fuselage
GB	=	gearbox
GT	=	gas turbine
max	=	maximum
miss	=	nominal mission, ex. reserves
$P1$	=	primary propulsor(s)
$P2$	=	secondary propulsor(s)
SL	=	sea level

DHEP	=	distributed hybrid electric propulsion
DoH	=	degree of hybridization, defined as $E_{bat_{nominal\ mission}}$ / $E_{total_{nominal\ mission}}$
SFC	=	specific fuel consumption
GT	=	gas turbine
HEA	=	hybrid electric aircraft
HEP	=	hybrid electric propulsion
HT	=	horizontal tail
ISA	=	International Standard Atmosphere
KPI	=	key performance indicator
LEDP	=	leading-edge distributed propulsion
MLM	=	maximum landing mass
MTOM	=	maximum takeoff mass
OEI	=	one engine inoperative
OEM	=	operational empty mass
PCP	=	power control parameters
SL	=	sea-level
T/O	=	takeoff
PREE	=	payload range energy efficiency
SP	=	specific power
SMR	=	short-medium range
SPPH	=	serial/parallel partial hybrid
TLAR	=	top-level aircraft requirement
TMS	=	thermal management system
VT	=	vertical tail

I. Introduction

IN ORDER to abide by the ambitious plans to reduce CO_2 emissions per passenger kilometer by 75% (relative to new aircraft in 2000) [1], the electrification of flight is one of the potential technological pathways. Such aircraft are envisioned to use electrical energy in their powertrain, eventually complemented with chemical energy, in which case they are called hybrid electric aircraft (HEA). The latter hybrid option appears relevant for the electrification of regional aircraft since the heavier battery of full-electric configurations may restrict their implementation to shorter ranges.

Interest in more electric, fully electric, and hybrid electric aircraft over the past decade has led to a vast amount of research and associated literature, produced by research institutes around the globe. The primary objective of this paper is not to provide an overview of the state-of-the-art, since many review papers exist that

Received 19 January 2024; accepted for publication 29 January 2025; published online 4 April 2025.

*Post-Doctoral Fellow, Flight Performance and Propulsion, Faculty of Aerospace Engineering.

†Assistant Professor, Flight Performance and Propulsion, Faculty of Aerospace Engineering; m.f.m.hoogreef@tudelft.nl. Senior Member AIAA (Corresponding Author).

cover a variety of perspectives. However, this section provides a short overview of (review) papers to support interested readers in their search of suitable references. This overview is by no means exhaustive.

Six types of hybrid electric powertrain layouts were proposed by Felder [2] and later adopted by the National Academy of Sciences [3]: conventional, series, parallel, turbo-electric, partial turbo-electric, and series/parallel partial hybrid. These differ in the coupling of the electric components with a combustion engine and thereby also differ in their working principle. For an extensive overview of the various technologies to enable hybrid-electric aircraft, including an overview of challenges and solutions, covering power electronics, energy storage, powertrain architectures, and electric motors/generators, we refer the reader to the work of Salem et al. [4]. Additionally, an overview of battery technology for more electric aircraft can be found in [5]. More details on the specific challenges in power electronics are provided by Radomsky et al. [6] and on electric drives by Sayed et al. [7]. The work of Brelje and Martins [8] provides an overview of the various concepts and models used for electric and hybrid electric aircraft, and Cardone et al. [9] provide an overview of recent developments specifically for HEA. The work of Viswanathan et al. [10] presents an overview of the challenges and opportunities associated with battery-powered flight.

In addition to the initial sizing method for hybrid-electric aircraft [11] that will be used in this paper, Orefice et al. [12], Finger et al. [13], and Cinar et al. [14] present similar methods. A number of authors from various institutions have developed methods to complement traditional conceptual aircraft design. For example, Pornet et al. [15,16] and Isikveren et al. [17] provide conceptual design approaches for hybrid-electric and dual-energy aircraft, respectively. Stückl [18] presents a detailed overview of the electric powertrain sizing for conceptual aircraft design, and Chakraborty and Mavris [19] explain a method for including novel subsystem design (e.g., electrified powertrains) in the early stages of aircraft design.

Energy management is another important topic for dual-energy powertrains such as HEA. Perullo and Mavris [20] present a review of energy management strategies for hybrid electric aircraft and how this could be included in initial aircraft sizing. Lee et al. [21] extend this to also include the flight path trajectory optimization in combination with optimization of the power split between battery and fuel energy.

Most design studies investigate the potential benefit of an HEA over a conventional (combustion) architecture by comparing their respective performance solely over their design mission (or harmonic mission) for an identical set of top-level aircraft requirements (TLARs) (e.g., [16,22–31]). But the majority of missions actually flown are less demanding in terms of payload and/or range than the design mission that sizes most components of the aircraft, as illustrated in Table 1 from the International Council on Clean Transportation report on CO_2 emissions from commercial aviation in 2013, 2018, and 2019 [32].

From Table 1, it can be observed that the typical operating point of regional (in the report, aircraft such as the Embraer E series, Dash 8-400, ATR72-600, and Canadair CRJs) and narrow-body (primarily the Airbus A320 family and Boeing 737 family) is well within their typical design point. Naturally, operational flexibility leverages this operating bandwidth, yet it indicates that the relative performance of HEA should be compared over the entire spectrum of the operating bandwidth of a particular design.

Therefore, better insight into the relative flexibility achievable by HEA is required. This will be the focus of this paper. In the present context, flexibility should be understood as the ability to perform efficiently, relative to a conventional aircraft (designed for the same design point!), for missions with a broad range of flight distances while carrying various amounts of payload. In contrast to a conventional design, where fuel mass is adapted to the mission payload and range, HEA may need to carry a battery of a given capacity and mass for all missions (although it may not be technically unfeasible to develop modular battery packs). Therefore, if a battery of given capacity and mass (as sized for the design point of the aircraft) must be carried on all missions, it is important to understand its consequences on off-design performance. The battery usage must therefore be adapted to various off-design missions to avoid penalizing energy and fuel consumption.

Table 1 Average distance flown per aircraft class in 2019, including their % of global total CO_2 emissions (data from Graver et al. [32])

Aircraft class	Average distance, km	% of global total CO_2 emissions
Regional	551	7
Narrow body	1322	51
Wide body	4675	42
Total	**1378**	**100**

For the hybrid electric powertrain architectures that do not involve a battery, such as the turbo-electric or partial turbo-electric architectures, large aeropropulsive benefits, leveraging improvements in the combination of propulsive and aerodynamic efficiency, are required from the distributed-electric propulsion to achieve substantial fuel burn reductions [33]. It is therefore chosen in this study to focus on battery-equipped HEA under the hypothesis that their off-design performance benefits from already installed battery capacity and on the corresponding powertrain architectures: parallel, serial/parallel partial hybrid (SPPH), and serial.

Existing works analyzing off-design performance focus on a retrofit of an existing aircraft for only one (parallel) hybrid electric powertrain architecture [34,35], on the off-design performance of a single (parallel) hybrid electric powertrain architecture [36], or only a single off-design mission [15] (with a different design mission for hybrid and combustion aircraft). However, to properly understand the performance of HEA, with a fixed battery mass based on the design point, on off-design missions (as flown in a realistic operating scenario), it is important to compare its flexibility relative to a conventional kerosene aircraft that is designed according to the same design point and performing the same off-design mission. The present paper's contribution is in the comparison of this relative flexibility of the aforementioned battery-assisted powertrain architectures. The starting point is the same as in other papers—a parallel hybrid electric powertrain architecture. This is subsequently extended to both the serial and SPPH powertrains.

A simplified analysis using some form of a range equation for hybrid electric aircraft, e.g., [37], could be used for off-design analysis. However, this does not capture the intricacies of the limiting aspects in the off-design operation of a hybrid electric powertrain. Therefore, the present paper is aimed at illustrating the powertrain characteristics throughout the operational envelope and using these characteristics to the maximum effect for off-design performance of HEA.

The structure of this paper is the following: Section II describes a design and analysis framework for aircraft conceptual design, including validation cases, with a particular focus on the necessary fine-tuning for HEA and the rationale for off-design mission analysis. Section III presents the aircraft sizing results for the various HEAs analyzed in this paper. Section IV presents the off-design performance results in comparison to conventional kerosene aircraft designed for the same design point and performing the same off-design mission. This section starts with an analysis of the limits caused by the powertrain characteristics of HEA in the payload-range diagram when flying off-design missions. The latter is important since for HEA the payload-range diagram is limited not only by the trade-off between payload and fuel mass for range but also by the different design points of the powertrain components. Section V presents the conclusions of the research and offers inspiration for future work.

II. Methodology

A. Aircraft Design Framework

The Aircraft Design Initiator (or, in short, Initiator) framework has been used in this research. The Initiator is an in-house-developed, automated design synthesis tool at the Flight Performance and Propulsion section of the Faculty of Aerospace Engineering at Delft

University of Technology. The synthesis process follows a convergence over several disciplinary analyses, typically based on handbook methods (e.g., [38–40]), empirical data, and physics-based methods (such as Engineering Sciences Data Unit (ESDU)). The Initiator was first developed as part of the European project Aerodesign (FP7) and has supported other European projects such as RECREATE (Horizon 2020), Smart Fixed Wing Aircraft (Clean Sky I), Parsifal (Horizon 2020), NOVAIR (Clean Sky 2—Large Passenger Aircraft), and CHYLA (Clean Sky 2—thematic topic). It has been under continuous development since. A description of the Initiator can be found in Ref. [41], and recent validation studies can be found in Ref. [42].

The Initiator can be used to assess the impact of small and large changes to the aircraft on the so-called key performance indicators (KPIs) in the conceptual design of FAR/CS 23 and FAR/CS 25 aircraft, supporting both propeller-powered and turbofan-powered aircraft, hybrid electric aircraft (with distributed propulsion), as well as conventional tube-and-wing aircraft, blended-wing–body aircraft, and box-wing aircraft. To do this, the Initiator synthesis relies on a convergence process. Hence, the aircraft is iteratively updated until a predefined set of KPIs (e.g., MTOM, tail size) converges below a prescribed threshold. This process of design "feasilization" [43] does not perform an actual optimization but tries to achieve a feasible design around the top-level requirements.

1. *Aircraft Sizing Process*

The Aircraft Design Initiator framework consists of a series of disciplinary analyses and sizing processes arranged into three main, partially nested, convergence loops (see Fig. 1). Note that Fig. 1 only shows the process on an aggregate level; many analyses actually consist of smaller methods. For example, "Geometry Estimation" contains more than 20 individual modules determining the aircraft geometry.

The first loop starts with a constraint analysis, tailored to hybrid electric aircraft, followed by a powertrain model. The constraint analysis derives, from the combination of a user-specified set of top-level aircraft requirements and performance requirements from regulations (FAR/CS 23/25), the required power and wing size using a typical constraint analysis in a wing versus power loading diagram. These form the inputs to a convergence around a mission and performance analysis and class I weight estimation. This iteration is necessary to resolve the sizing of the hybrid electric powertrain components (particularly the battery) and weight estimation dependencies.

In the next step, the geometry of the aircraft is generated, following an inside-out aircraft design process using also empirical sizing rules and user-specified input on the aircraft configuration. Based on this geometry, the aircraft operational empty mass is estimated using the method from Torenbeek [38], and the aerodynamic properties are estimated using a vortex-lattice method complemented by a parasite drag estimation based on Torenbeek [38], Roskam [39], Obert [40], and ESDU methods. An updated mission analysis (and energy carrier sizing) is performed with the updated empty mass to update the maximum takeoff mass. The system masses and the aircraft aerodynamic properties are then fed back to the start of the loop until their differences with the previous iteration fall below a certain threshold.

In the third loop, "Class-II.5 weight estimation" includes a semi-analytical fuselage weight estimation method ([44–47]) and a finite-element-based wing weight estimation [48] to incorporate the effects of distributed propulsion on the structure. This includes landing loads and 2.5G pull-up at both maximum zero fuel and maximum takeoff weight.

2. *Powertrain Modeling*

Part of the Initiator developments has been the modification to include also HEA and fully electric aircraft based on the work by de

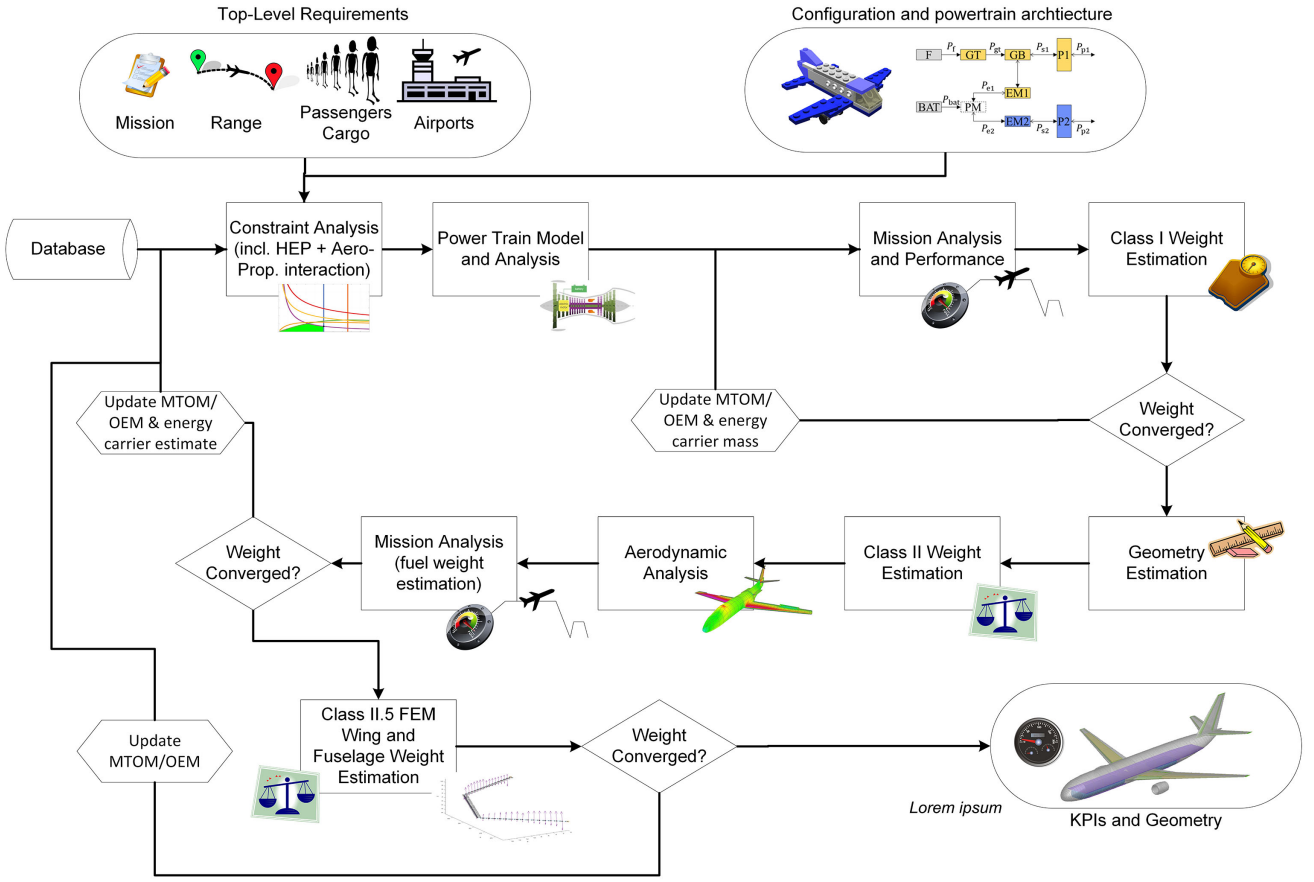

Fig. 1 Initiator flowchart. Adapted from Hoogreef et al. [25] with permission. Reprinted with permission from [25]. Copyright ©2020 by Maurice F. M. Hoogreef, Reynard de Vries, Tomas Sinnige, and Roelof Vos. Published by the AIAA, Inc., with permission.

Vries [11,49] (which was later validated in [50]). For the representation of the powertrains, a simplified model is used, following the six layouts proposed by Felder [2] and later adopted by the National Academy of Sciences [3]: conventional, series, parallel, turbo-electric, partial turbo-electric, and series/parallel partial hybrid.

The powertrain architecture modeling (illustrated in Fig. 2 for battery-assisted hybrid electric powertrains) considers a primary and secondary chain, including primary ($P1$, coupled to the gas turbine —GT) and secondary propulsors ($P2$, electrically driven) to also allow modeling distributed propulsion with multiple types of engines. Depending on the powertrain architecture, up to three so-called *power control parameters* (PCP), defined in Eqs. (1–3), can be necessary to determine the power flow (indicated by P) within each component. Note that the conventional kerosene powertrain would follow by simply removing all battery (BAT) and electric components from the parallel or SPPH chain. Fuel is indicated by F, a gearbox by GT, and the power management module by PM. EM1 and EM2 indicate the electrical machines of the primary and secondary chain, respectively.

The *supplied power ratio* (see [17,51]) is expressed as the ratio of battery-supplied power to the total supplied power.

$$\phi = \frac{P_{\text{bat}}}{P_{\text{bat}} + P_f} \tag{1}$$

The second power control parameter is the *shaft power ratio*, defined as the ratio of the mechanical shaft power supplied to the secondary propulsion layout to the total shaft power produced by the powertrain.

$$\varphi = \frac{P_{s2}}{P_{s1} + P_{s2}} \tag{2}$$

Finally, the *gas turbine throttle* parameter, expressed in Eq. (3), represents the power fraction at which the GT is operating, as the ratio of the produced power to the maximum power it can produce in the given flight condition.

$$\xi = \frac{P_{\text{GT}}}{P_{\text{GT,max}}} \tag{3}$$

The gas turbine performance is not modeled in detail in this conceptual aircraft design study. Instead, the engine efficiency is determined per time instance and per flight phase of the mission analysis (also for off-design missions) using a modification of Eq. (13.9) from Raymer [52], and the density lapse with altitude is also taken into account for the amount of power that is available. This equation relates throttle setting to thermal efficiency. This efficiency is used in the powertrain analysis based on [11] to compute the amount of fuel required. The baseline gas turbine thermal efficiency is computed from an estimated specific fuel consumption (SFC) for the reference aircraft.

Electrical component masses are determined using gravimetric power/energy densities for all components in the chain (electromotors, generators, inverters, and power electronics) and follow the approach of a "combined specific power" based on the specific power (SP) of each component as presented in Ref. [33]. Here, a distinction between motors and generators is made in the mass estimation, and an "equivalent specific power," which combines the electrical machine and associated transformer, is used. This provides a "black box" approach, suitable for conceptual sizing that provides a simplified, top-level understanding of the effects of powertrain technology levels, which is independent of the particular design of the electrical system, as it does not require information regarding every component in the powertrain. An additional 30% mass penalty is added to account for additional power distribution and cooling aspects.

The power loading of all powertrain components is sized by adjusting the power control parameters (PCP) in each required flight constraint. One key flight constraint is the cruise, which we use to size the GT: the GT should be able to sustain the required cruise propulsive needs at a certain throttle setting, together with the battery-supplied power ratio set at the required hybridization value, and should not be oversized by any other constraints. The battery power loading is then adapted such that it can support the GT in satisfying all other required flight constraints (sizing for power).

3. *Mission Analysis*

The aforementioned power control parameters (ξ, ϕ, and φ) are also considered in the mission analysis, which is implemented as a point model—a time-step summation over the mission, using the control laws. This equates a power balance across the entire (hybrid) propulsion system, instead of a range equation approach. From the power balance, the energy consumption can be determined per component of the powertrain (in a way that is also suited to kerosene aircraft). The model assumes constant component efficiencies per analysis, except for the gas turbine (GT), which is a function of the GT throttle ξ.

The PCP must be determined by the user for each flight phase of the mission analysis (and can differ for the beginning and end of each phase). The powertrain model is adapted for each flight phase to calculate the power/energy balance. Consider, e.g., the difference between active components in the powertrain of the same aircraft with a kerosene engine that is electrically boosted (parallel in Fig. 2) for the takeoff phase and pure kerosene combustion in the cruise phase ($\phi = 0$).

In other words, once the sizing of all components is obtained (Sec. II.A.2), it is still possible to adapt the PCP for the various segments of both the nominal and the diversion mission (sizing for energy). In both cases, we ensure that we do not exceed the sizing (in terms of power) of any component. Similarly, in both cases, the

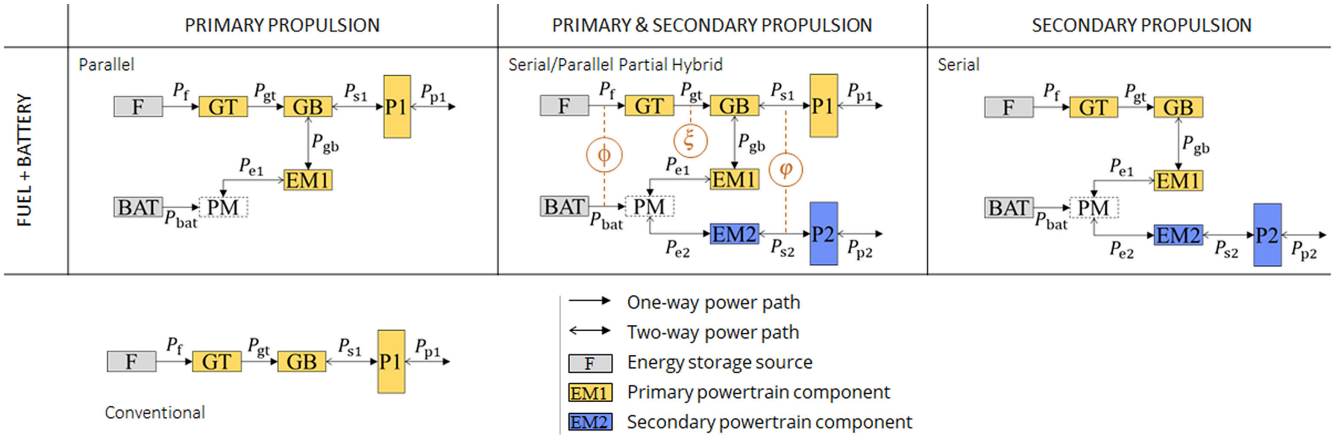

Fig. 2 Powertrain architectures and power control parameters for battery-assisted hybrid electric powertrains.

mission analysis determines the required battery (and fuel) capacity and hence its mass, which has implications on the whole aircraft design.

4. *Fine-Tuning Power Control Parameters*

Power control parameters (Sec. II.A.2) can be set to different values for different flight phases, such that climb can use a different power split compared to cruise or descent. By affecting the power-related sizing within each branch of the powertrain (i.e., impacting the power loading in a typical constraint diagram that forms the starting point of the aircraft design process [see, e.g., Fig. 1]) and the energy required along the mission, those power control parameters have a significant impact on design. A discussion of the impact of PCPs on the various hybrid electric architectures is provided in [4].

In our previous design studies (e.g., [25,53]), the battery was designed to minimize the gas turbine (GT) sizing by providing power during some design constraint and was used during the mission along a reduced period of time (e.g., climb) in order to limit the mass penalty associated with a larger capacity. During the mission cruise, the GT throttle ξ was set at a value of 90%, and the battery-supplied power ratio ϕ was left to be determined. Practically speaking, this would result in the battery providing a few percent of power at maximum during the heaviest part of the cruise and then lowering to no power toward the end of the cruise phase. Consequently, the resulting HEA performed poorly compared to their conventional counterpart.

It is now understood that there is more potential in leveraging the high efficiency of the electric drivetrain (compared to the primary powertrain) than in the marginal increase in GT power-loading or in aeropropulsive benefits. Therefore, this study is conducted by choosing a different PCP strategy: a positive constant supplied power ratio $\phi^* > 0$ is prescribed along the mission cruise phase, with the GT throttle left undetermined. On top of that, for the cruise constraint, the couple (ϕ_{cr}, ξ_{cr}) is set at $(\phi^*, 0.90)$ and ϕ is adapted for all other design constraints to ensure that the GT is sized by the cruise constraint. Effectively, during cruise, the GT throttle found to maintain cruise conditions is hence around 0.90, which ensures maximum GT efficiency. This iterative procedure must be repeated for any new design.

In a nutshell, the GT is effectively downsized to its cruise condition, with the battery complementing it for other design constraints, and the battery provides a constant positive ϕ^* during cruise. This design choice seemed rather appropriate, even though optimality is not proven, and provides the advantage of being systematically applicable to various designs, therefore providing a common sizing approach for all battery-equipped aircraft studied. This enables to compare various HEA designs on the sole basis of their different powertrain architectures. Besides, for all the aircraft studied, the emphasis is therefore placed on the selection of ϕ^*, which can be understood as the degree of hybridization of the cruise phase. Furthermore, for all designs, specific care is given to not oversize powertrain components: the PCPs are heuristically adapted for each constraint of the diagram to ensure that each component reaches their highest power-loading values. Once again, optimality is not proven, but that approach has shown merits by allowing us not to penalize a given design through oversizing one of its powertrain components.

It should be noted that with a higher ϕ^*, the GT power loading increases, and the GT may not be powerful enough to cover the aircraft propulsive needs entirely during energy-demanding diversion phases, such as loiter and diversion cruise. In such cases, the GT must be complemented by some battery by setting the battery-supplied power ratio positive for those mission phases, which therefore requires a larger battery capacity to cope with those non-nominal flight segments. The difference between nominal and diversion is that, in the latter case, we voluntarily limit the battery usage to its strict minimum. Consequently, especially for HEA with a high degree of hybridization, additional battery capacity is required to perform loiter or diversion segments. This additional mass is accounted for in the iteration between sizing for power and sizing for energy.

Additionally, care must be taken to ensure sufficient power for any inoperative (OEI) scenario (one engine or critical powertrain component). These conditions are for this study evaluated during the constraint analysis (Fig. 1), following the approach by de Vries et al. [11]: "OEI is interpreted here as the failure of any one component of the powertrain. An exception is the PMAD, which is assumed to contain redundant buses such that the failure of a component of the primary powertrain branch does not affect the secondary powertrain branch and vice versa. Thus, the effect of a single component failure can be accounted for by oversizing all components of the branch where the failure occurs by a factor $N_1/(N_1 - 1)$ or $N_2/(N_2 - 1)$, depending on whether the failure occurs in the primary or secondary powertrain branch, respectively."

The shaft power ratio φ affects the thrust share between the primary and secondary powertrain. With increasing φ, the distributed propulsion gets allocated a higher thrust, and therefore eventual aeropropulsive benefits (such as reduction in induced drag) can be more pronounced. However, it also affects the sizing of components of the secondary powertrain and, depending on the powertrain architecture, can be associated with higher power conversion losses. In fact, for the SPPH powertrain, the lowest powertrain mass can be achieved by having zero conversion between primary and secondary chain when sizing for energy (effectively, $P_{e1} = P_{gb} = 0$ in Fig. 2). An analytical equation can be derived to achieve this condition [Eq. (4)], as illustrated in Fig. 3. Even though this latter condition does not guarantee an optimum design (especially if the distributed propulsion entails aeropropulsive benefits), it was heuristically shown to minimize powertrain mass and power conversion losses. This arbitrary balance of power was therefore selected for the SPPH powertrain architecture.

$$\phi = \frac{\varphi \cdot A_\eta}{1 + \varphi \cdot (A_\eta - 1))} \tag{4}$$

$$A_\eta = \frac{\eta_{GT} \cdot \eta_{GB}}{\eta_{PM} \cdot \eta_{EM2}} \tag{5}$$

5. *Off-Design Mission Analysis*

The mission analysis strategy, adopted from De Vries et al. [11], allows exploration of off-design missions once an aircraft has been sized. This allows determining the required fuel and battery energy to perform a mission different from design and thereby determine off-design degrees of hybridization. To perform such an off-design analysis, the mission analysis is adapted to reevaluate any provided mission specification under the following constraints:

1) The onboard battery mass (determined during on-design sizing) cannot be exceeded.

2) The maximum tank volume (determined during geometrical sizing for the design mission) cannot be exceeded.

3) The maximum takeoff mass of the aircraft cannot be exceeded.

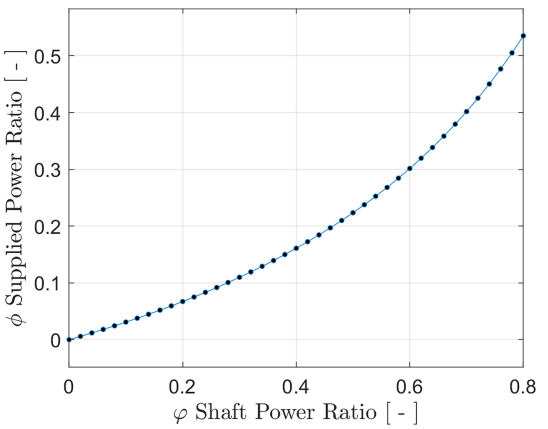

Fig. 3 Relation between φ and ϕ to ensure zero conversion between primary and secondary powertrains of an SPPH architecture.

4) The maximum landing mass of the aircraft cannot be exceeded.

5) The maximum payload mass cannot be exceeded (consequently, the maximum zero-fuel mass cannot be exceeded).

6) The operative empty mass is fixed.

7) The drag polar of the aircraft is predetermined (only reevaluated to account for the current mass, i.e., required lift, and trim of the aircraft).

8) Propulsive efficiency curves for the different propulsors are fixed.

9) Installed power of any powertrain component cannot be exceeded.

Off-design mission specifications allow a full description of the mission profile (for any number of off-design cases), including number of passengers, payload mass, cruise speed and altitude, range, diversion range, and loiter time. Additionally, the aircraft configuration (clean, landing gear extended or retracted, and/or flaps extended or retracted) can be specified per phase to allow full flexibility.

The key difference for (hybrid-)electric off-design analysis is the additional flexibility over the powertrain settings (PCPs) during any of the flight phases of any off-design mission, under the constraint that installed power or battery energy cannot be exceeded. Moreover, different constraints from different powertrain components become active to limit the payload-range capability of the hybrid electric aircraft. This will be explained in a case study in Sec. IV.A.

Once an aircraft has been sized, the exploration of off-design missions serves a twofold objective:

1) Identify the payload-range capabilities of a given HEA, also known as the payload-range diagram.

2) Determine performance figures for any mission within the payload-range diagram.

In the remainder of this study, off-design studies are conducted by only varying payload and range and leaving cruise speed and altitude unchanged compared to the design mission. Similarly, requirements related to diversion and loitering are also left unaltered. If that choice is made for the sake of simplicity, it should be noted that, for mission ranges inferior to the design range, lowering the cruise altitude and the cruise speed accordingly is likely to yield a higher energy efficiency. Another important assumption is that it was decided to maintain the battery-supplied power ratio constant throughout the whole cruise phase. The eventual benefits related to varying the battery-supplied power ratio along cruise were deemed of second order and neglected in the present context for the sake of simplicity. Finally, power control parameters were also left unchanged for the climb and descent segment, as well as for loiter and diversion segments.

6. *Payload-Range Diagram*

To identify the envelope of feasible missions in payload-range coordinates, the maximum range must be found for each payload value. For a conventional aircraft, this is done by trading payload against extra fuel (at constant MTOM). However, for HEA, to each payload corresponds a different value in battery-supplied power ratio in cruise (ϕ^*) that maximizes the range: payload is also traded against fuel at constant MTOM such that ϕ^* must then be lowered to fly a longer cruise segment without exceeding the battery capacity. On the other hand, lowering the supplied power ratio requires to accordingly increase the GT throttle to maintain the same propulsive power, such that a lower limit on ϕ^* also exists. For each payload, the ϕ^* value that maximizes range is found heuristically:

1) The range is increased step by step.

2) For each candidate range value, minimum and maximum values for ϕ^* are identified by running the corresponding mission analysis and testing the constraints mentioned above in Sec. II.A.5.

3) The difference between the maximum and minimum value narrows with an increasing range such that the maximum range is reached when those become equal.

7. *Performance Map*

Using the above iterative process, the maximum flyable range (and corresponding ϕ^* value) is found for every payload value down to zero (ferry flight scenario) to eventually give shape to the envelope of all feasible missions. The second objective of the exploration of off-design missions is to map the aircraft performance over this space of feasible missions. The strategy to maximize off-design performance of the HEA set in this paper was to maximize ϕ^* so as to leverage the available battery capacity. Contrary to fuel, for which the onboard mass can be varied, the HEA always carries its full battery mass, such that off-design missions are performed with the highest efficiency if the PCPs make full use of it. In the same fashion as the process described in Sec. II.A.6, for each mission considered, the highest allowable value ϕ^* is found heuristically by increasing it step-by-step until one of the constraints listed in Sec. II.A.5.

B. Aircraft Design Framework Validation

The analysis methods and synthesis process of the Initiator framework are regularly benchmarked against data from the open literature, and comparisons are typically presented with every publication (e.g., [25,41,42]). Additionally, a separate comparison of the preliminary sizing method for HEA [11] is performed by Finger et al. [50].

The regional aircraft designs considered in the present study require some correction factors of the Initiator to be calibrated to match a reference turboprop aircraft and (hybrid-)electric study aircraft. These calibrations are performed to match gas turbine efficiency (since no detailed engine model is included) to correct secondary and nonoptimal mass estimations of the class II.V methods for fuselage and wing (to correct the "ideal" primary structure required to withstand the loads) and a calibration of the drag polar (excrescences). The resulting comparisons against the ATR72-600 and Piaggio E-STOL are presented in this section.

1. *Validation of Regional Turboprop Design*

As the focus of this paper is on regional propeller aircraft, a conventional tube-and-wing reference configuration with wing-mounted propellers is chosen. The ATR72-600 was selected as the reference aircraft and, according to its specifications, was designed using the Initiator. The top-level aircraft requirements (TLARs) for the ATR72-600 have been derived from publicly available data.

The resulting performance, dimensions, and masses are compared to values found in open literature in Table 2. It can be noted that the differences, after calibration of drag polar and corrections for nonoptimality of the structural mass estimation for fuselage and wing, are well within the bandwidth that is typically expected for conceptual aircraft design. The largest difference is found in terms of the gas turbine power loading, which may be attributed to an overestimation of the propeller performance in takeoff and climb conditions. For the present study, this is considered acceptable as the

Table 2 Comparison of KPIs for the reference regional aircraft and its Initiator sizing, after calibration

Parameter	Unit	ATR72-600[a]	Initiator ATR72-600	Δ, %
Wing loading, W_{TO}/S	kN/m^2	3.70	3.66	−0.93
GT power loading, $W_{TO}/P_{GT,\,max,\,SL}$	N/W	$5.5 \cdot 10^{-2}$	$5.1 \cdot 10^{-2}$	−6.91
OEM fraction, OEM/MTOM	— —	$5.85 \cdot 10^{-1}$	$5.90 \cdot 10^{-1}$	0.94
OEM	t	13.5	13.6	1.09
MTOM	t	23.0	23.0	0.14
S	m^2	61.0	61.7	1.15
b	m	27.0	27.2	0.74
l_{fus}	m	27.2	27.8	2.17
d_{fus}	m	2.87	2.78	−3.14
Fuel consumption[b]	kg/h	650	656	0.90

[a]Data from Jane's "All the world's aircraft" and ATR 72-600 Fact sheet: https://www.atr-aircraft.com/wp-content/uploads/2020/07/Factsheets_-_ATR_72-600.pdf [retrieved 8 Nov. 2023].

[b]This results in a baseline specific fuel consumption of 294 g/kW/h, which will be used for all case studies. Engine thermal efficiency is varied as explained in Sec. II.A.2.

Table 3 Comparison of KPIs for the Piaggio E-STOL and its Initiator sizing (note that nominal mission values do not include reserves)

Parameter	Unit	Piaggio E-STOL[a]	Initiator E-STOL	Δ [%]
Wing loading, W_{TO}/S	kN/m^2	3.38	3.38	−0.12
GT power loading, $W_{TO}/P_{GT,max,SL}$	N/W	$1.14 \cdot 10^{-1}$	$1.15 \cdot 10^{-1}$	0.88
Battery power loading, W_{TO}/P_{bat}	N/W	$7.80 \cdot 10^{-2}$	$7.70 \cdot 10^{-2}$	−1.28
E-motors power loading, W_{TO}/P_{EM2}	N/W	$6.30 \cdot 10^{-2}$	$5.90 \cdot 10^{-2}$	−6.38
OEM (exc. bat) fraction, OEM/MTOM	— —	$4.63 \cdot 10^{-1}$	$4.75 \cdot 10^{-1}$	2.58
Block fuel fraction, $M_{f,miss}$/MTOM	— —	$6.20 \cdot 10^{-2}$	$6.20 \cdot 10^{-2}$	−0.43
Battery mass fraction, M_{bat}/MTOM	— —	$3.13 \cdot 10^{-1}$	$3.08 \cdot 10^{-1}$	−1.68
OEM (exc. bat)	t	5.92	6.04	1.97
MTOM	t	12.8	12.7	−0.69
Fuel energy (nominal mission)	GJ	33.8	33.5	−0.83
Battery energy (nominal mission)	GJ	3.93	3.99	1.63
DoH (nominal mission)	%	10.4	10.7	2.21
S	m^2	37.1	36.8	0.81
b	m	24.4	24.2	0.83
l_{fus}	m	16.4	16.6	1.22

[a]Data obtained/computed from [54–56] and communication with the authors of [56].

same estimate for propeller performance will be used for both kerosene and hybrid designs. The aforementioned calibration will be maintained for the analysis of HEA in this paper.

2. Validation of (Hybrid-)Electric Aircraft Design

A further validation case is presented in Table 3 based on open literature on a 19-seater hybrid electric commuter aircraft: the Piaggio *E*-STOL (as presented in [54–56]). The aim of this case study is to demonstrate the performance of the hybrid electric sizing methods integrated in the Initiator design framework, with the same technology scenario (as used in Sec. III.A) as used for the *E*-STOL. This technology scenario will be used for the HEA design and off-design analysis in this paper.

Similar to the conventional turboprop aircraft, all parameters are well within the bandwidth expected for conceptual aircraft design. In this case, the largest difference is found for the power loading of the electromotor on the secondary chain (EM2). Since, in fact, the *E*-STOL is using a serial architecture, it is the secondary chain that provides the propulsive power. Hence, this is again impacted by the same modeling of propeller performance in takeoff and climb conditions as for the ATR72-600, and the error is in the same order of magnitude. An updated propeller model (suitable for conceptual aircraft design) is under development and is expected to reduce these differences in the validation cases. However, this difference is not expected to significantly impact the trends observed in the rest of this paper. Therefore, this (small) difference in power loading is accepted.

III. Aircraft Sizing Results

This section details the baseline aircraft designs that are used for the off-design performance analysis in Sec. IV. A description is given of the top-level aircraft requirements (TLARs) (Sec. III.A) used to size all aircraft, as well as the technology scenario that is used for the HEA. Section III.B presents the aircraft sizing results for the baseline kerosene and battery hybrid electric aircraft.

A. Top-Level Aircraft Requirements and Technology Scenario

The TLARs for the baseline kerosene and hybrid electric aircraft designs have been derived from publicly available data[‡§¶] of various regional propeller transport aircraft for the CHYLA project.[**] These TLARs describe a typical operational scenario for regional turboprop aircraft in terms of payload, range, and runway requirements. The cruise Mach number was specifically selected on the lower end of the performance spectrum during the requirement specification phase of the CHYLA project. Table 4 presents the top-level aircraft requirements.

Table 4 Top-level aircraft requirements for all regional aircraft designs

Requirement	Unit	Value
Passenger capacity	— —	70
Maximum payload	kg	7500
Harmonic range	km	926
Cruise Mach number	— —	0.4
Cruise altitude	m	7010
Landing distance	m	1006
Takeoff distance	m	1372
Diversion range	km	185
Endurance	min	45
Diversion Mach number	— —	0.28
Diversion altitude	m	1500
Climb performance	— —	17.5 min to 5400 m

The technology assumptions made for the present study are listed in Table 5. These are aligned with the EU battery technology roadmap for the 2030–2035 timeframe and the Clean Sky 2 Small Air Transport transversal activity.

B. Baseline Aircraft Sizing Results

The baseline aircraft designs consist of four different configurations, with two variants per hybrid electric powertrain architecture, resulting in a total of seven baseline aircraft. Because of the different components present in the different hybrid powertrain architectures, the aircraft also differ in their propulsion system layout. However, all share the same configuration in terms of fuselage, wing, empennage, and landing gear. Both the kerosene and parallel architecture feature a conventional single propeller. The serial hybrid aircraft has two gas turbine generators that drive a layout of six distributed propellers positioned in-board. Six distributed propellers were considered a promising configuration that does not suffer from debilitating mass penalties in earlier research [25], and it realizes a compromise between propeller disk loading (and thus propulsive efficiency) and powertrain mass. The SPPH aircraft has two main propellers and six smaller distributed propellers positioned near the wingtip. The four different aircraft configurations are presented in Fig. 4.

[‡]https://janes.ihs.com/JAWADevelopmentProduction.
[§]https://www.flyfokker.com.
[¶]https://www.atr-aircraft.com.
**CHYLA—Credible HYbrid eLectric Aircraft: https://cordis.europa.eu/project/id/101007715.

Table 5 Electric components assumptions, aligned with EU battery roadmap[a] and Clean Sky 2 Small Air Transport[b]

Parameter	Unit	Value	Remark
Battery gravimetric energy density (pack level)	Wh/kg	340	Corresponds to a used battery of initial density 400 Wh/kg. Corresponding cell-level value is 600 Wh/kg.
Battery volumetric energy density (pack level)	Wh/L	800	— —
Battery minimum state-of-charge	%	20	— —
Electromotors gravimetric power density	kW/kg	3.77	Includes motor (6.70 kW/kg for axial flux permanent magnets direct drive motor). DC/AC converter (18 kW/kg) and cooling systems (0.85 kW/kg) for both. Heat rejection assumed 5% and 1% of input power for motor and DC/AC converter, respectively.
Electro generators gravimetric power density	kW/kg	4.79	Includes generator (11.96 kW/kg for permanent magnet synchronous generator), AC/DC converter (18 kW/kg), and cooling systems (0.85 kW/kg) for both. Heat rejection assumed 4% and 1% of input power for generator and AC/DC converter, respectively.
Electromotors volumetric power density	kW/L	18.2	Electric drive only, excludes eventual gearbox.
Battery DC/DC gravimetric power density	kW/kg	14.85	Includes DC/DC converter (18 kW/kg) and cooling system (0.85 kW/kg, with 1% assumed heat rejection.
Battery TMS gravimetric power density	kW/kg	0.36	Dissipates battery heat to the outside.
Battery heat rejection	%	3	Fraction of battery power output dissipated as heat.

[a]https://battery2030.eu/research/roadmap/.
[b]https://cordis.europa.eu/project/id/945500.

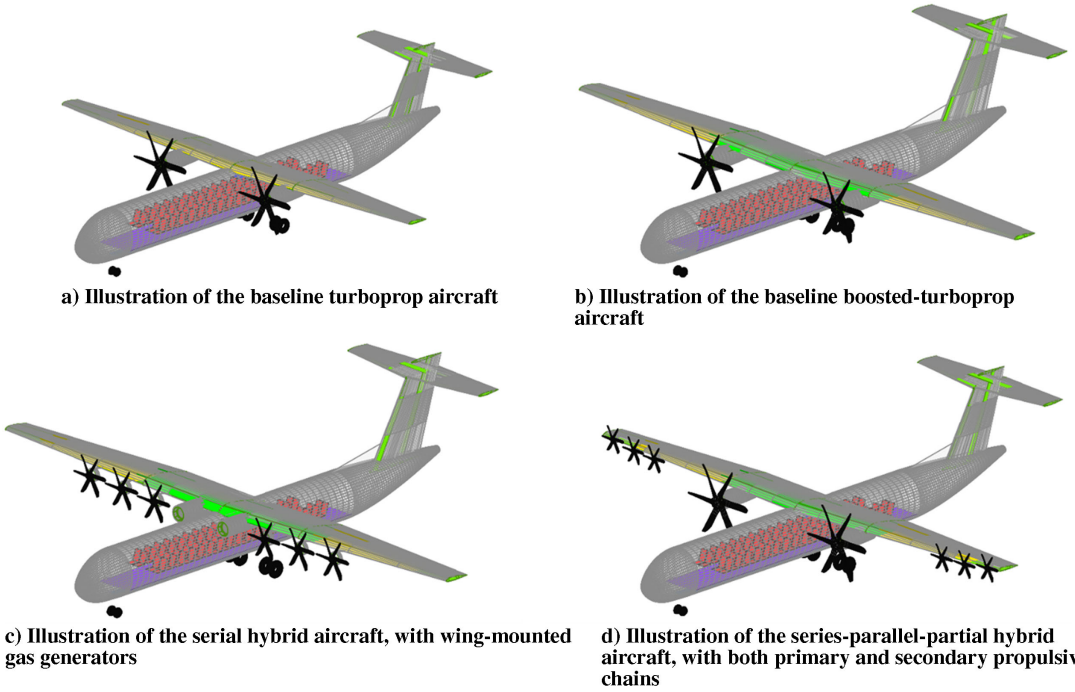

a) Illustration of the baseline turboprop aircraft

b) Illustration of the baseline boosted-turboprop aircraft

c) Illustration of the serial hybrid aircraft, with wing-mounted gas generators

d) Illustration of the series-parallel-partial hybrid aircraft, with both primary and secondary propulsive chains

Fig. 4 Notional pictures of the various regional designs. Only $\varphi = 10\%$ hybrid-electric variants are shown. Variants with $\varphi = 20\%$ are similar but larger due to increased MTOM.

The results of the baseline aircraft sizing according to the TLAR from Table 4 and the technology scenario according to Table 5 are shown in Table 6 for all four powertrain architectures (seven total baseline designs). For all HEA, two variants were sized: one for $\phi^* = 10\%$ and one for $\phi^* = 20\%$.

A clear hierarchy in HEA performance emerges from this preliminary design study: serial HEAs are outperformed by parallel boosted turboprops, themselves outperformed by SPPH configurations. This trend concerns all aspects: for a given payload and harmonic range, the better configuration would offer the lightest MTOM (hence likely the lowest cost solution), the highest efficiency (and hence the lowest energy costs), and the lowest block fuel burn (and hence the lowest emissions), and would be less exposed to a span limit. Such a span limit may be constraining for hybrid-electric aircraft, also in terms of battery volume in the wing [57]. In fact, both the serial and parallel HEA with $\phi^* = 20\%$ already exceed the ICAO type C gate limit of 36 m, which indicates that $\phi^* = 20\%$ is an upper hybridization limit for the configurations and set of TLARs considered in this study.

Both SPPH aircraft are even able to outperform the baseline kerosene aircraft in terms of fuel energy required to perform the mission even though both aircraft are significantly heavier than the kerosene alternative. Although the SPPH HEAs still have slightly higher average SFC, they have significantly lower GT power and mass as they leverage the effects of distributed propulsion (as will be discussed in the next paragraph). However, in terms of total energy consumption, the kerosene aircraft still consumes slightly less than the hybrid electric alternatives. The SPPH HEA, as well as the serial HEA, also achieves slightly higher wing loading due to the aero-propulsive benefits of the distributed propulsion that is enabled by these powertrain architectures.

If we compare the power loading values obtained for the three architectures, e.g., for $\phi^* = 10\%$, we can clearly see the performance advantage of the SPPH architecture over the others. Since the

Table 6 KPI comparison for kerosene and hybrid-electric aircraft sized with Initiator (N.B. EM1 is operating as electric motor for parallel hybrid and is thus sized accordingly in terms of power density)

Parameter	Unit	Kerosene baseline	Parallel hybrid ($\phi^* = 10\%$)	Parallel hybrid ($\phi^* = 20\%$)	Serial hybrid ($\phi^* = 10\%$)	Serial hybrid ($\phi^* = 20\%$)	SPPH ($\phi^* = 10\%, \varphi = 30\%$)	SPPH ($\phi^* = 20\%, \varphi = 50\%$)
W/S	kN/m^2	3.66	3.66	3.66	3.99	3.99	3.92	3.94
$W_{TO}/P_{GT,\,max,\,SL}$	N/W	$5.10 \cdot 10^{-2}$	$8.91 \cdot 10^{-2}$	$1.24 \cdot 10^{-1}$	$8.51 \cdot 10^{-2}$	$1.23 \cdot 10^{-1}$	$8.46 \cdot 10^{-2}$	$1.24 \cdot 10^{-1}$
W/P_{EM1}	N/W	— —	$9.03 \cdot 10^{-2}$	$7.26 \cdot 10^{-2}$	$9.41 \cdot 10^{-2}$	$1.31 \cdot 10^{-1}$	1.59	2.07
W/P_{EM2}	N/W	— —	— —	— —	$6.04 \cdot 10^{-2}$	$6.04 \cdot 10^{-2}$	$2.07 \cdot 10^{-1}$	$1.22 \cdot 10^{-1}$
P_{GT} (total)	MW	4.33	3.83	3.71	4.57	4.15	3.62	3.11
P_{EM1} (total)	MW	— —	3.78	6.34	4.13	3.91	0.19	0.19
P_{EM2} (total)	MW	— —	— —	— —	6.44	8.45	1.48	3.17
MTOM	t	22.5	34.8	46.9	39.6	52.1	31.2	39.5
OEM	t	13.3	25.4	37.4	29.9	42.3	22.0	30.4
M_{wing}	t	2.22	3.67	5.22	4.17	5.68	3.06	4.01
M_{fus}	t	2.49	2.61	2.97	2.65	3.14	2.61	2.71
$M_{powertrain}$	t	2.18	3.11	3.83	5.44	6.04	2.58	3.14
$M_{elec.\,prop.\,chain}$	t	— —	1.04	1.67	3.44	4.22	0.65	1.40
$M_{comb.\,prop.\,chain}$	t	2.18	2.07	2.16	1.99	1.82	1.93	1.74
M_{EM1} (each)	t	— —	0.52	0.84	0.43	0.41	0.02	0.02
M_{GT} (each)	t	0.51	0.45	0.44	0.53	0.49	0.43	0.37
M_{EM2} (each)	t	— —	— —	— —	0.28	0.37	0.07	0.14
$M_{f,\,miss}$	t	1.75	1.90	2.00	2.30	2.29	1.70	1.60
M_{bat}	t	— —	8.54	16.8	9.76	18.4	6.62	12.6
$E_{f,\,miss}$	GJ	50.4	51.9	51.5	62.3	57.8	47.4	41.2
E_{bat} (nominal mission)	GJ	— —	7.03	13.9	8.12	15.3	5.65	10.6
DoH (nominal mission)	%	— —	11.9	21.3	11.5	20.9	10.7	20.5
SFC (cruise average)	g/kW/h	289	291	291	291	291	290	290
l_{fus}	m	27.7	27.7	27.7	27.7	27.7	27.7	27.7
d_{fus}	m	2.77	2.77	2.77	2.77	2.77	2.77	2.77
S	m^2	60.3	93.3	126	97.4	128	78.1	98.4
b	m	26.9	33.5	38.8	34.2	39.2	30.6	34.4
d_{P1}	m	3.91	4.09	4.09	— —	— —	4.46	4.95
d_{P2}	m	— —	— —	— —	2.44	2.80	1.60	2.73

GT is sized for the same cruise conditions for the same battery-supplied power ratio in all three cases, the obtained GT power loadings are very similar. However, EM1 in the SPPH case is, respectively, 18–19 times smaller (relatively) than for the parallel and serial case. Because there is a primary propulsor on the SPPH, the power loading of EM2 is also considerably higher than for the serial case (three-and-a-half times higher). Overall, for the SPPH, the combined power loading of EM1 and EM2 is five times higher than for the serial case.

The debilitating impact of the degree of hybridization on mass can be clearly understood here, with HEA easily exceeding twice the mass of the baseline aircraft, despite a cruise ϕ^* limited to 20% on their harmonic mission. The minimum MTOM increase over the baseline is around 50% for the parallel SPPH aircraft of low cruise supplied power ratio $\phi^* = 10\%$. Note that, in general, the SPPH aircraft are significantly lighter than their serial or parallel counterparts with identical ϕ^*.

This conclusion may seem counterintuitive as the SPPH architecture is the most extensive hybrid powertrain that contains the most components and nodes. However, this design architecture enables to minimize the power loading of the EM1, which has, by essence, the role of an intermediate between the primary and secondary branches of the powertrain. In serial or parallel powertrains, the presence of a single propulsion layout requires EM1 to be either sized by the maximum GT power output case (serial) or by the battery maximum power output case (parallel). In an SPPH architecture, the primary and secondary branches can be maintained quasi-independent, and therefore EM1 can be relatively small.

The relatively small size of EM1 is also synonymous with limited power conversion during mission phases, which drastically reduces conversion losses (even though a rather high efficiency value of 0.95 is assumed for EM1). Therefore, the payload range energy efficiency (PREE) advantage of SPPH configurations (for a given ϕ^*) over other HEAs would even increase with increasing design range (as is illustrated in the Appendix). The design objective for SPPH HEA should thus be to minimize EM1 in order to avoid a mass penalty.

IV. Off-Design Performances

A. Parallel Hybrid Aircraft

Before analyzing the off-design sensitivity of the various battery support hybrid electric powertrain architectures, it is important to highlight the key differences between the payload-range diagrams of a conventional (kerosene) and HEA. This section illustrates those differences through the example of a parallel hybrid electric regional aircraft compared to a kerosene regional turboprop, and it is concluded by a comparison of the approach to that of Palaia and Abu Salem [36], who perform an analysis on the off-design performance of the parallel hybrid architecture as well.

The payload-range diagrams of both aircraft are shown in Fig. 5; the design mission is displayed by the yellow dot, and the value of the maximum achievable battery-supplied power ratio in cruise is

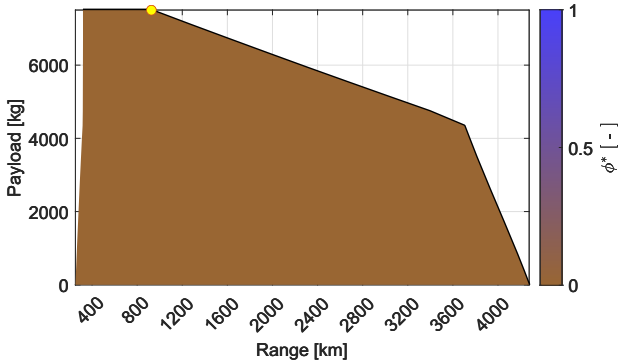

a) Payload-range diagrams of "Conventional" aircraft

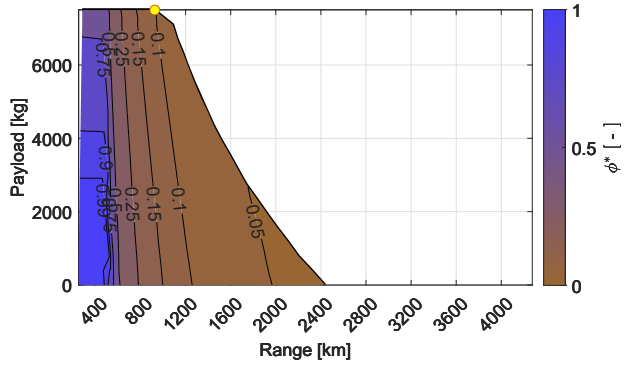

b) Payload-range diagrams of parallel hybrid aircraft ($\phi^* = 10\%$) with contours of maximum battery-supplied power ratio during cruise

Fig. 5 Payload-range diagrams of "conventional" and parallel hybrid aircraft. The yellow dot corresponds to design mission, which is identical for both aircraft.

displayed via colored contours. For the conventional aircraft, the battery-supplied power ratio is trivially null (no battery) such that the payload-range domain is uniformly covered with the corresponding brown color. Note that, in this example, the battery-supplied power ratio for the design mission of the hybrid electric aircraft is set to $\phi^* = 10\%$.

Upon inspection of Fig. 5, the most striking difference is naturally the difference in achievable ferry range. The ferry distance is nearly halved, and the slope after the first kink (next to the design point) is steeper. Overall, a significant domain of missions that can be covered by the conventional aircraft is not within the capabilities of the HEA. It concerns the vast majority of missions beyond the design range, for which only a fraction can be flown by the HEA at a cost of a significant payload reduction.

Secondly, as may be expected, the hybridization of the cruise phase (in this case shown through the supplied power ratio ϕ^*) is increasing exponentially when moving to smaller ranges. At the lowest ranges, an additional increase of ϕ^* can be observed with reducing payload. This highlights that range sensitivity over payload sensitivity of these HEA.

One important difference compared to the classical case is the shape of the diagram envelope. For the classical diagram, where initially payload is traded for extra fuel until the tanks are full, and later payload is reduced to fly even further, a quasi-linear behavior that is well-known from aircraft design literature can be observed. However, in the case of the HEA, this corresponding part of the diagram is not linear. This is illustrated in more detail in Fig. 6.

Figure 6 illustrates the same payload-range diagram of the same parallel HEA as shown in Fig. 5. However, this time, two sets of missions of the diagram [in (a) and (c)] are shown (dotted black curves), together with the evolution of certain design KPIs, relatively to their maximum design values, along those missions. This choice of display was made to comparatively track how KPIs vary in both cases in order to understand what the limiting factors are for the payload-range diagram and explain the shape of the second kink observed in the former diagrams. In (a) and (b), missions follow the payload-range diagram external envelope; it is expected to find a limiting factor for all those missions. In contrast, in (c) and (d), missions start at half the maximum payload and concern all ranges up until the maximum allowable range at that payload. Then those missions also follow the envelope of the payload-range diagram, such that the values of KPIs displayed in (b) and (d) are to be identical part of this maximum range. In (b), three characteristic range values are displayed in green to support the following explanation.

Considering the set of missions in (a) and (b), point A marks a first step. Below that range, the battery output power in cruise (discharge rate limited) is at its maximum permitted value and consequently limits ϕ^* to values around 60%. It should be noted that for the design mission (yellow dot, corresponding to point B), for which $\phi^* = 10\%$, the battery output power is at only ~30% of its maximum permitted value. During this initial part of the diagram, the gas turbine throttle is very low ($\xi \sim 0.13$) as the battery provides most of the power in cruise conditions [$\phi^* \sim 60\%$ as can be seen in (a)]. Below the flight range at point A it can also be seen that the battery energy is not used up to full capacity because the discharge rate is at its maximum over the cruise flight segment. As range increases, the battery gets used to a higher fraction of its energy capacity until it eventually reaches 100% of used capacity in point A. Over that same domain, as the range increases while the GT power rating is quasi-steady (nonzero since it must complement the battery that outputs its maximum power), the fuel mass therefore increases, but only marginally because the battery provides the majority of power. Consequently, the TOM increases slightly, which explains why the GT power output is near constant but slightly increasing.

Beyond the flight range at point A, the battery energy is used at full capacity, such that the battery power output must be reduced to further increase range. This requires the gas turbine to complement the power deficit by suddenly working at higher throttle values for flight ranges beyond point A, with a corresponding increase in fuel mass to complement the battery capacity over longer missions. The payload stays constant at its maximum value until the TOM reaches MTOM in point B.

Beyond the flight range at point B, similar to the classical case, payload mass is traded for fuel mass such that the TOM stays at MTOM. The battery power output needs to decrease further to supply the full battery energy capacity despite the range increase. The GT throttle consequently increases to compensate for the decreasing battery power output until it eventually reaches its maximum in C. Therefore, the propulsive power output in cruise can only decrease beyond the flight range of point C: the battery power output is limited by the battery capacity (energy) sizing and the GT power output by the GT sizing. To further increase mission range, the TOM must therefore be reduced via a sharper reduction in payload. This decrease in payload beyond point C continues until the ferry mission case is reached. It should be noted that, at this point, the battery-supplied power is not null: it cannot be decreased further because the GT operates at its maximum power rating and would not be able to meet the cruise power requirements without some power complement from the battery. Besides, the fuel mass is getting close to its maximum but does not reach it; otherwise, a fourth kink point in the payload-range diagram would have been present.

The sizing of powertrain components impacts the limits of the payload-range diagram. The flight range of point B can only increase by changing the harmonic range, but the range at point C can increase if the GT power loading is decreased. For the current study case, the GT throttle in cruise for the design mission (yellow dot) was set at 90% for the sake of a high GT power loading and maximum GT efficiency in cruise. This means that the GT is already rather close to its maximum power output in cruise for the design mission. Lowering the throttle setting ξ_{cruise}

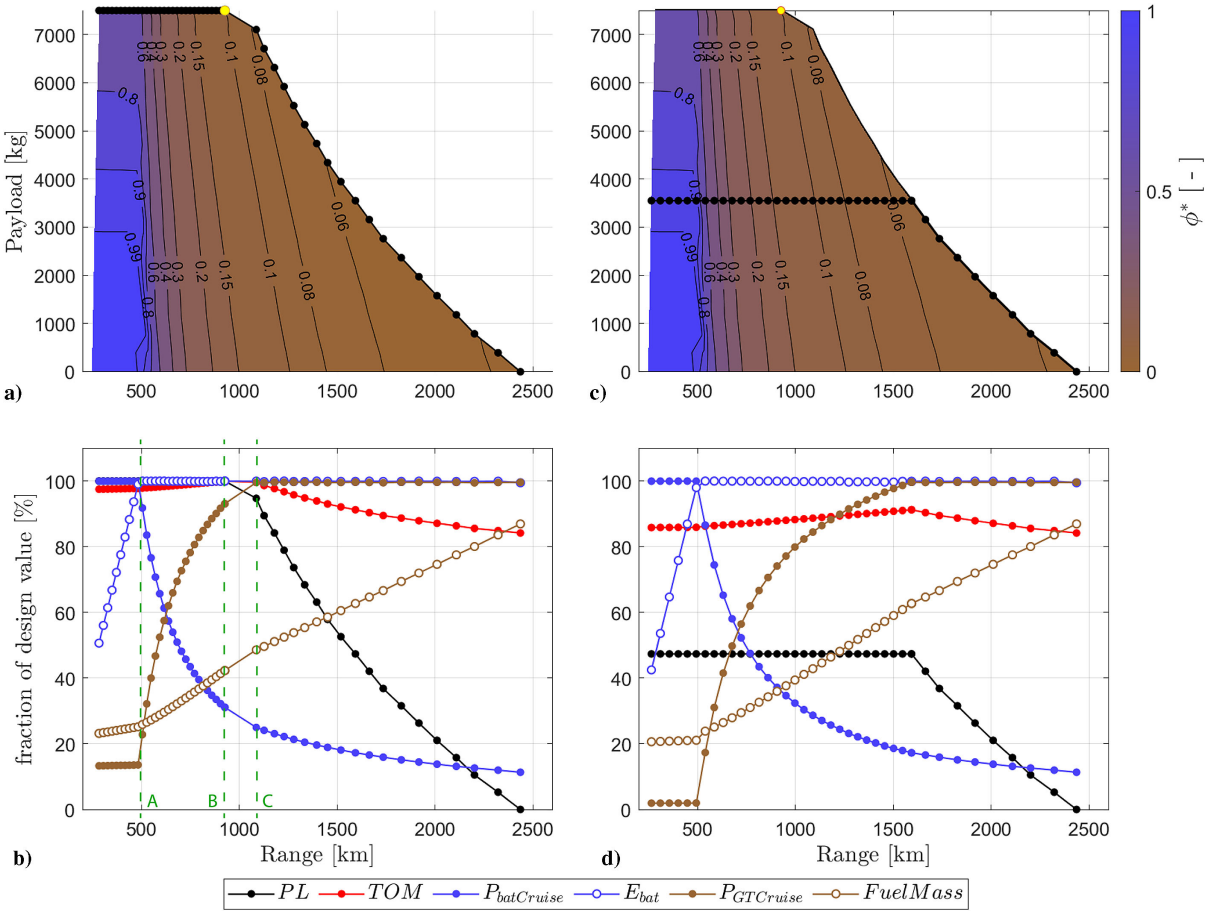

Fig. 6 Set of missions represented on payload-range diagrams for maximum payload (a) and half payload (c) together with the evolution of their respective power and energy variations, relative to their maximum values [in (b) & (d)].

would have a marginal impact on GT efficiency but would enable to enlarge the payload-range diagram at the expense of a heavier GT.

In Figs. 6c and 6d, a mission at reduced payload is simulated. It can be seen that the limit cases in the powertrain look relatively similar. Due to the lower payload, the maximum takeoff mass is not reached. Thus, the gas turbine power output can be significantly lower, hence increasing the hybridization in short missions. This is illustrated by the much higher ϕ^* until ~500 km. This also causes the slope of the fuel consumption to be lower initially.

Points *B* and *C* are moved much further right and coincide. This occurs at the point where the GT is at maximum throttle and battery power output is limited by the battery capacity. At this point, the limit of the payload-range diagram is reached (as identified before), and range can only be decreased by a TOM reduction (sharper reduction in payload). This decrease in payload again continues until the ferry mission case is reached, which is limited by the powertrain rather than the fuel tank capacity.

All in all, the payload-range diagram of this parallel hybrid aircraft (with a fixed battery mass/capacity) is therefore much more restricted than that of a conventional aircraft. The ferry range is more than twice as low, and the shape of the payload-range diagram has a much more pronounced nonconvexity due to the different powertrain limitations.

Palaia and Abu Salem [36] also perform an off-design mission analysis of a parallel hybrid regional aircraft. Although the aircraft studied in that paper is slightly smaller, the trends seen are comparable in terms of cruise phase electrification potential (for points with lower range/payload than the design point). In that sense, the present work (as will be explained in the next section) is complementary to [36] by expanding the off-design analysis to the other battery-supported hybrid powertrains (series and SPPH).

It should be noted that Palaia and Abu Salem [36] perform an analysis of the payload-range diagram from a different perspective. Whereas, in the present paper, the battery mass determined during the sizing of the aircraft is considered to be a fixed component installed in the wing, Palaia and Abu Salem [36] consider different cases of trading fuel, battery, and payload mass. These may offer potential for range extension when battery swapping is possible. Nevertheless, similar to our conclusion shown in Fig. 6, the authors of [36] conclude that part of the payload-range diagram may become limited by the thermal power of the combustion engine.

Figure 7 illustrates the same payload-range diagram of the parallel HEA with $\phi^* = 10\%$ together with two additional contour plots. Next to the variation of the battery-supplied power ratio in cruise are shown the relative difference in PREE with a kerosene aircraft sized for the same design mission and evaluated over the same off-design mission and the relative difference in fuel consumption with respect to the aforementioned kerosene aircraft. The bottom-most fraction of the PREE plot is white because of the low payload resulting in a very small value (due to the nominator of the equation becoming small) and the heavy hybrid aircraft requiring significant energy (denominator increasing).

An interesting observation from Fig. 7 is that the area of highest supplied power ratio in cruise does not necessarily correspond one to one to the region of highest efficiency improvement or largest reduction in fuel burn. On the contrary, in terms of PREE, a local optimum seems to be present at about a sixth of the design payload and slightly below the 600 km range. Naturally, this region also

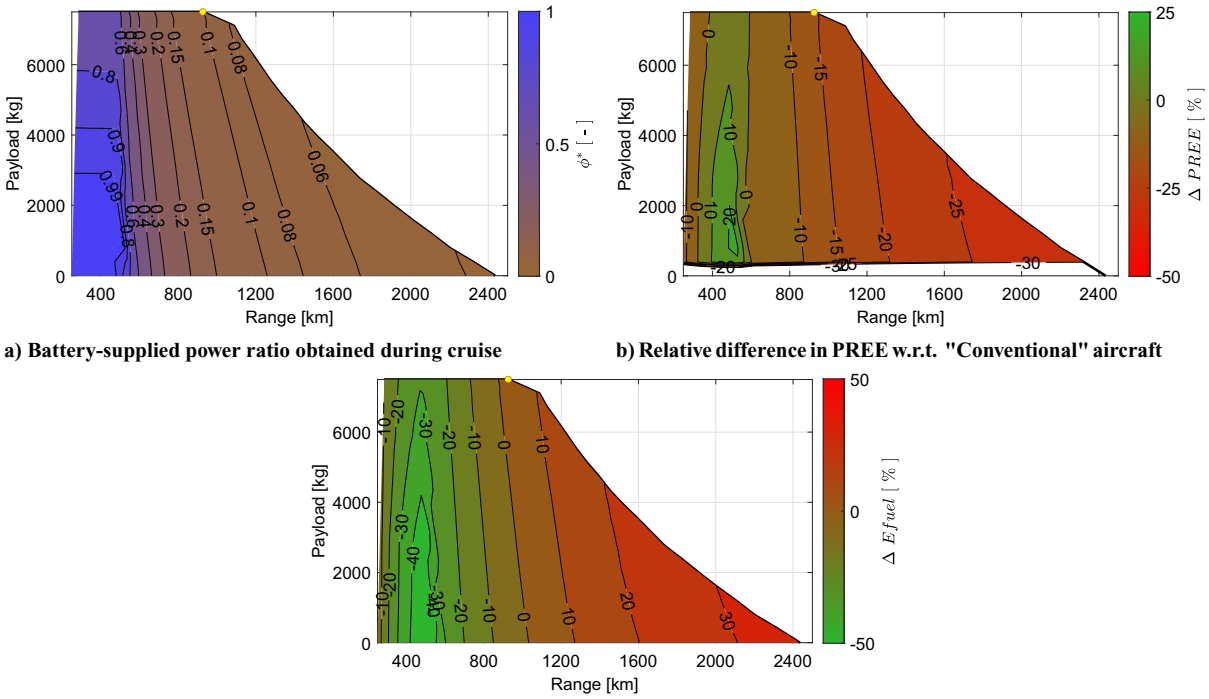

a) Battery-supplied power ratio obtained during cruise

b) Relative difference in PREE w.r.t. "Conventional" aircraft

c) Relative difference in nominal mission fuel burn w.r.t. "Conventional" aircraft

Fig. 7 Payload-range diagram of a parallel HEA with $\phi^* = 10\%$ displayed with various contours.

corresponds to the highest fuel burn reduction of up to 50%. The reason that the lowest range sees the highest electrification but not the highest efficiency is that for smaller ranges the cruise segment gets relatively shorter compared to the climb and descent segments. Therefore, as soon as the battery-supplied power ratio in cruise reaches a plateau with decreasing ranges, the overall efficiency starts to decrease.

The delta fuel burn contour, however, shows an interesting development in comparison to the PREE. Already slightly below the design point, the hybrid electric aircraft requires less fuel to perform the mission even though the PREE is still much worse than the kerosene aircraft (around 10% worse). The heavier aircraft (by nature) requires more energy to perform the mission, and hence its PREE is lower. However, it requires less fuel thanks to the hybridization. This illustrates one of the fundamental theses of this study: drawing prospective conclusions based on the sole analysis of the design mission can lead to overlooking the potential of HEA for off-design missions. In the case of the parallel HEA with $\phi^* = 10\%$, the fuel burn over the design mission is a few percent higher than the conventional aircraft. However, for lower ranges, such as the 551 km average distance flown by regional aircraft (Table 1), a hybrid electric aircraft with only $\phi^* = 10\%$ can achieve a benefit of approximately 30–50% in terms of fuel consumption depending on the payload.

Note that here a design with a capacity of 70 passengers was used, yet a larger payload capacity may be more beneficial for electrified aircraft as shown in [58] and demonstrated in the CHYLA project.[††] However, this means that the ICAO C-gate span limit of 36 m is sometimes exceeded, which can be a major operational concern for regional operations. An analysis of the sensitivity to design payload is presented in the Appendix, with the corresponding wingspan.

[††]CHYLA—Credible HYbrid eLectric Aircraft: https://cordis.europa.eu/project/id/101007715. Deliverable 3.3 Report on opportunities for cross-vehicle class and technology synergies: https://ec.europa.eu/research/participants/documents/downloadPublic?documentIds = 080166e5fbee16cc&appId=PPGMS.

Overall, this section has outlined that the payload-range diagram of HEA is determined by an intricate combination of sizing limits of powertrain components in terms of both power and energy. The electrification narrows the payload-range diagram significantly, and if further study cases can be envisioned (increasing gas turbine size), there seems to exist a pronounced trade-off between operational flexibility and operational efficiency. Within those restricted payload-range diagrams, the HEA can, however, reach interesting performance levels, such that comparing HEA and baseline on the basis of their design mission seems too restrictive. Ideally, aircraft are compared on a distribution of missions.

B. Design Exploration: Degree of Hybridization and Powertrain Architecture

The previous section demonstrated how the payload-range capability of a typical HEA is determined by the limits of the various powertrain components and how this impacts the operational performance of a parallel hybrid electric regional aircraft. However, the off-design performance of HEA can be expected to vary not only with classical TLAR (for the design point) in terms of payload and range but also with powertrain architecture and with the battery-supplied power ratio in cruise selected for the design mission. Therefore, this section will further detail the off-design performance of HEA by showing the parallel (boosted) hybrid turboprop next to the serial configuration and SPPH layout for both $\phi^* = 10\%$ and $\phi^* = 20\%$. The focus is on battery-equipped HEA, because their off-design performance may benefit from already installed battery capacity.

The variation of cruise supplied power ratio with payload and range for parallel, serial, and SPPH HEA is shown in Fig. 8 for design points with $\phi^* = 10\%$ and $\phi^* = 20\%$. The most noticeable difference between the left- and right-hand sides ($\phi^* = 10\%$ and $\phi^* = 20\%$, respectively) is the achievable ferry range. This is much less for the $\phi^* = 20\%$ due to the overall mass increase and the lower off-design ϕ^* reducing powertrain efficiency. However, the aircraft with a higher supplied power ratio on the design point (Fig. 8b) allows for full-electric cruise over a much

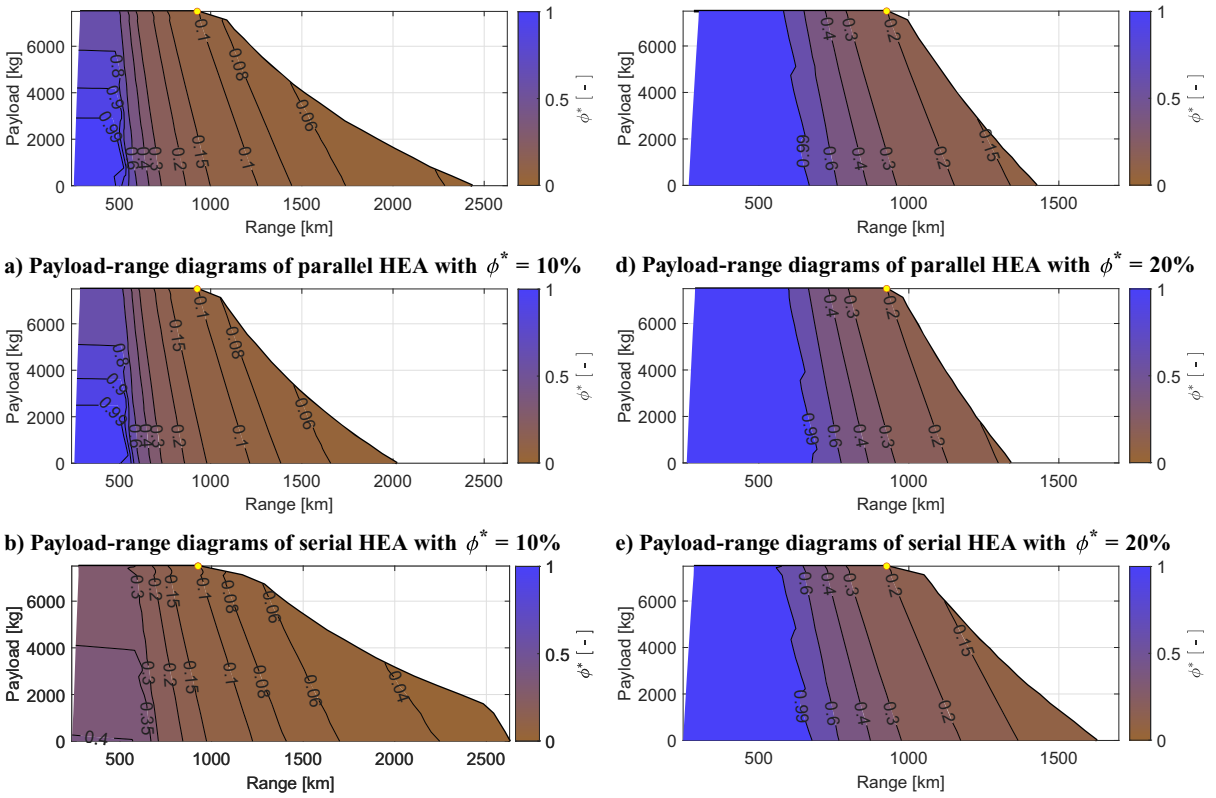

Fig. 8 Supplied power ratio contours in off-design payload-range conditions for six battery hybrid electric aircraft, designed for the same point (yellow dot).

larger domain. For $\phi^* = 10\%$, a clear difference between parallel and serial on one side versus SPPH can be noticed. The former two powertrain architectures are able to sustain full electric cruise over a larger domain of missions (although the serial architecture has the smallest range flexibility), contrary to the design point where SPPH is outperforming the other two in terms of mass and energy consumption (see Table 6). That can be explained by the fact that, for the SPPH, an increased battery power output (off-design) is directly related to a higher thrust on the smaller DP propellers driven by the electric drivetrain, which induces a lower propulsive efficiency. Therefore, the off-design performance map is also dependent on the distribution of disk area between the primary propulsor and the distributed propulsor. Hence, it will depend on propulsion layout and propeller design (the latter is not accounted for in this conceptual aircraft design study). For the design point $\phi^* = 20\%$, the supplied power ratio contours are much more similar for all architectures, and the SPPH actually allows the largest flexibility in terms of achievable range. For that level of hybridization, the shaft power ratio of the SPPH configuration was expected to be much higher, and the DP disk area was enlarged in anticipation. Another particularity concerns the shape of the payload-range diagram envelope of the SPPH designed for $\phi^* = 10\%$. A second kink can be observed at the 2500 km range (Fig. 8a, bottom), which is due to the fuel reaching its maximum tank volume. As discussed in the previous section, that limitation did not occur for the parallel HEA. For the SPPH with higher hybridization $\phi^* = 20\%$ (Fig. 8b, bottom), the maximum ferry range is reached before the fuel hits its maximum allowable volume, and the second kink is not present.

As can be seen in Fig. 9, the higher degree of hybridization allows the HEA designed with $\phi^* = 20\%$ on their harmonic missions to reach the largest block fuel reductions, as well as to extend the domain that sees a reduction in block fuel to a larger space of off-design missions. For the maximum payload over 600 km, the fuel burn reduction of the $\phi^* = 10\%$ is around 20%, while the $\phi^* = 20\%$ manage >40%.

Overall, the electrification narrows the payload-range diagram significantly, especially for the lowest payloads, with a nearly twofold reduction in ferry range. However, electrification also enlarges the domain of missions favorable to HEA, which concerns the fraction of missions of lower ranges. Incidentally, it is shown that the largest benefits are achieved, for the family of HEA designed in this study, near the 550 km average vector length of regional aircraft. For the lowest $\phi^* = 10\%$ hybridization value, the sharpest reduction in fuel burn for missions at maximum payload, $\sim -25\%$, is achieved by the parallel configurations. For higher $\phi^* = 20\%$ hybridization, the SPPH configuration achieves the highest reduction, $\sim -55\%$ in fuel burn. Overall, the SPPH configuration is able to leverage best on electrification on the harmonic mission, even though the added benefits of flying off-design are relatively lowest for this configuration. As above, a fine-tuning of the distribution of propulsive disk areas between primary and DP could improve it. Over the whole domain, SPPH still offers the most compelling compromise among hybrid configurations.

Figure 9 is indicative of the impact of the chosen design point in terms of both powertrain architecture and hybridization on the off-design performance. It clearly demonstrates the need to consider these architectural choices early on during the design of an HEA, on top of the classical TLAR (primarily payload, range, and flight speed). It also indicates that, depending on the hybridization that is chosen for the design point, the chosen architecture plays a distinct role for the off-design performance of such HEA. In fact, the architecture with the largest fuel saving (parallel) for $\phi^* = 10\%$ may not offer the best flexibility with range and may be outperformed by another architecture (SPPH) when the design point hybridization ($\phi^* = 20\%$) is increased, due to the nature of the

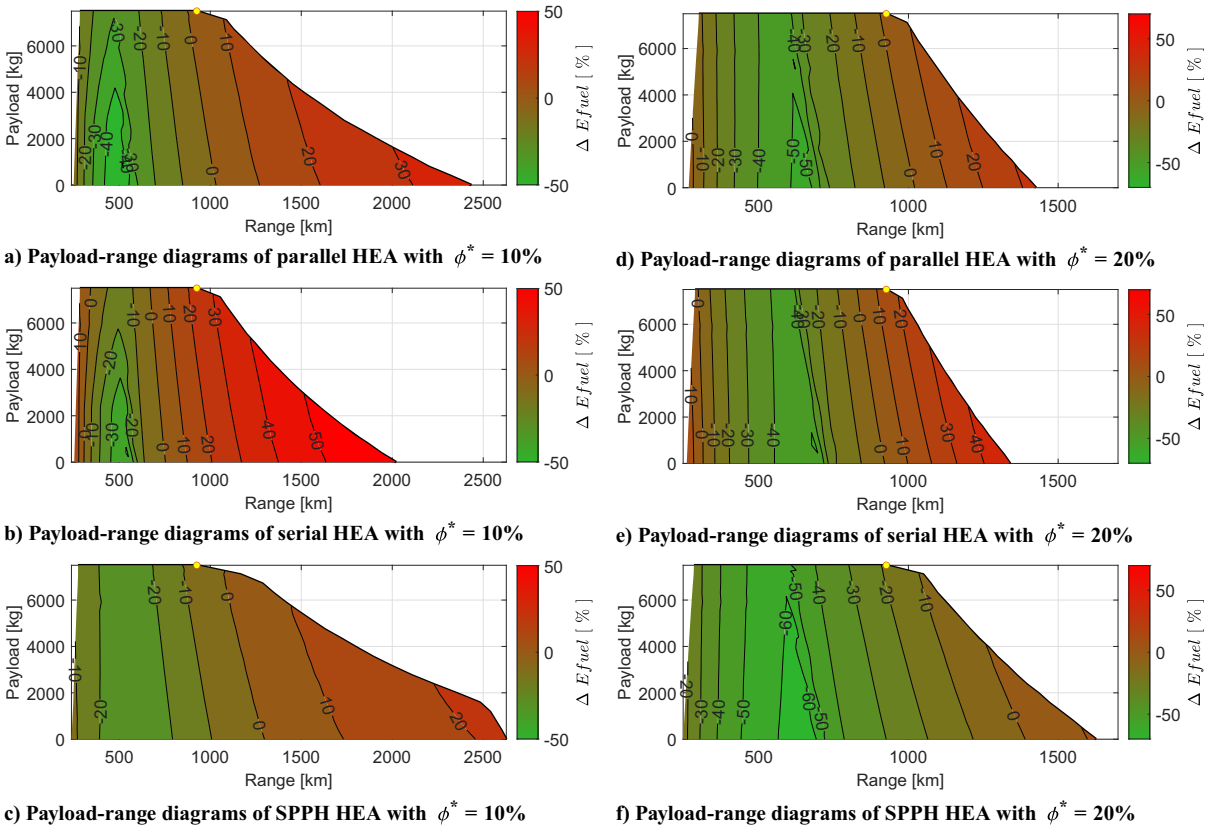

a) Payload-range diagrams of parallel HEA with $\phi^* = 10\%$

d) Payload-range diagrams of parallel HEA with $\phi^* = 20\%$

b) Payload-range diagrams of serial HEA with $\phi^* = 10\%$

e) Payload-range diagrams of serial HEA with $\phi^* = 20\%$

c) Payload-range diagrams of SPPH HEA with $\phi^* = 10\%$

f) Payload-range diagrams of SPPH HEA with $\phi^* = 20\%$

Fig. 9 Relative fuel burn contours in off-design payload-range conditions for six battery hybrid electric aircraft compared to a kerosene aircraft performing the same mission, designed for the same point (yellow dot).

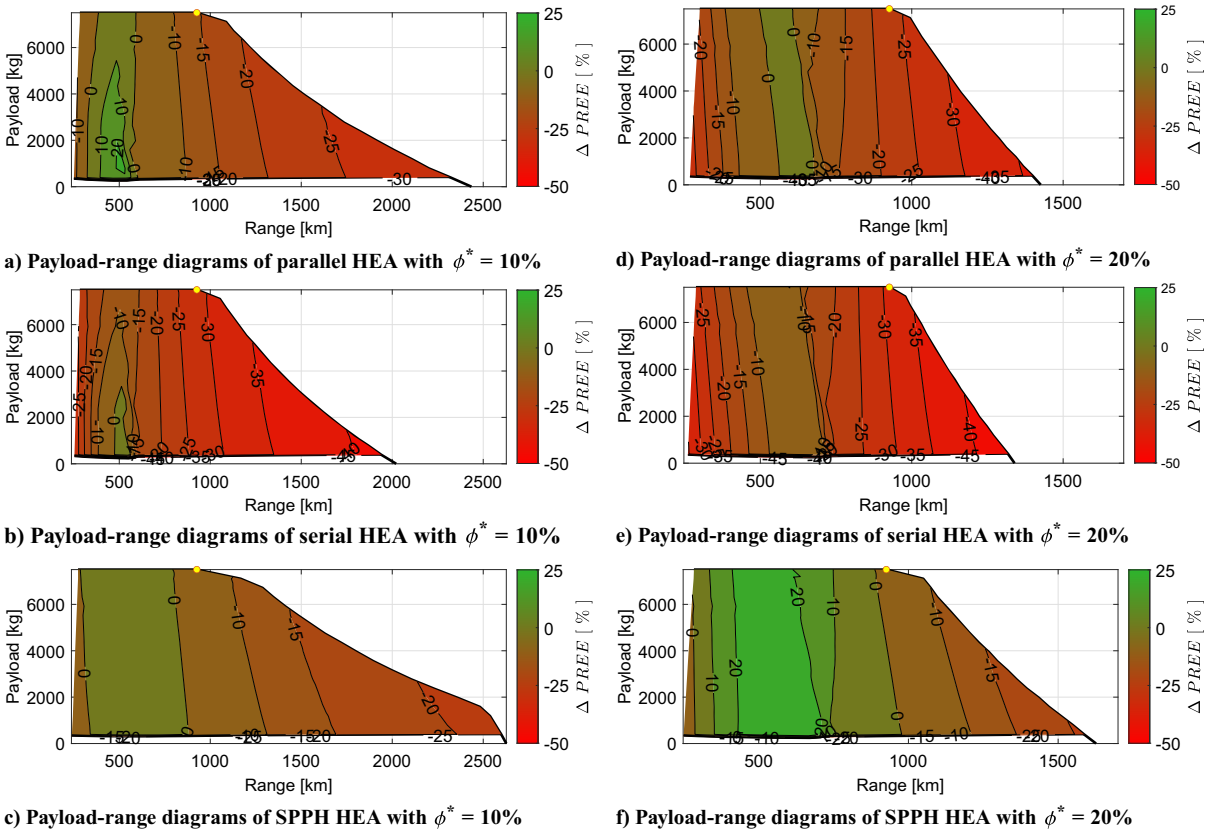

a) Payload-range diagrams of parallel HEA with $\phi^* = 10\%$

d) Payload-range diagrams of parallel HEA with $\phi^* = 20\%$

b) Payload-range diagrams of serial HEA with $\phi^* = 10\%$

e) Payload-range diagrams of serial HEA with $\phi^* = 20\%$

c) Payload-range diagrams of SPPH HEA with $\phi^* = 10\%$

f) Payload-range diagrams of SPPH HEA with $\phi^* = 20\%$

Fig. 10 Relative PREE contours in off-design payload-range conditions for six battery hybrid electric aircraft compared to a kerosene aircraft performing the same mission, designed for the same point (yellow dot).

powertrain component limitations. Note that a fuel saving on an off-design mission with respect to a kerosene aircraft, designed for the same mission, flying that same off-design mission, does not necessarily yield an increase in PREE. As demonstrated in Fig. 10, an increase in payload-range energy efficiency is only found in a much smaller area of the payload-range envelope. This is caused by the fact that the hybrid aircraft are heavier and therefore require more energy.

V. Conclusions

To assess the off-design capabilities of hybrid-electric flight, all three battery-equipped hybrid-electric configurations have been considered: parallel, serial, and SPPH. Two values in the battery-supplied power ratio during the cruise segment of the harmonic mission (ϕ^*) were used for each hybrid powertrain architecture, 10% and 20%, resulting in the design of six HEAs from a common set of TLARs. The same sizing approach was applied to all designs: the cruise segment sizes the GT, assuming a throttle of 90%, and the battery provides the necessary power complement for other required flight phases. For the SPPH design, the shaft power ratio between two distinctive set of propellers (GT driven and electrically driven) must be set. It was selected to ensure no transfer of power between the thermal powertrain and the electric one to reach higher power loading values and to lower power conversion losses. In comparison with a conventional design based on the same harmonic mission, none of the six HEA manages to reach the PREE of the conventional design, and only the SPPH enables to exhibit a lower fuel burn. The hierarchy with HEA is clear: based on the sizing approach and overall configuration chosen in this study, the SPPH design is lighter, more compact (less exposed to span-related gate constraints), and more efficient.

From those aircraft sized on the same harmonic mission, an off-design exploration is conducted with the objective to identify the payload-range envelope and to assess their performance for any missions within their respective payload-range capabilities. It was outlined that the payload-range diagram of HEA is determined by an intricate combination of sizing limits of powertrain components, in both power and energy. It means that the shape of the diagram is highly dependent on the hybrid powertrain architecture, as well as on the sizing of its components and there seems to exist a pronounced trade-off between operational flexibility and operational efficiency.

The effect of hybridization and powertrain architecture off-design performance was assessed. Both play an important role. A higher hybridization enlarges the array of missions that are favorable for HEA against conventional aircraft, at the price of a reduction in payload-range capabilities. The relative benefits (compared to on-design) of flying off-design are maximized by the serial configurations, which, however, starts with the highest penalty on the harmonic mission. Overall, the SPPH offers a rather compelling compromise among hybrid configurations over the whole diagram. Finally, the achieved fuel burn reduction when flying off-design is significant (up to 60% on some missions) for all hybrid configurations. In fact, all configurations with higher ϕ^* allow for full electric cruise up to ~500 km range, regardless of payload. These are concentrated around range values that are the most representative of regional operations, such that comparing HEA and baseline on the basis of their design mission seems too restrictive and should rather be done on the basis of a distribution of missions.

Appendix: Design Sensitivities of HEA to Payload and Range

This appendix presents the design sensitivities of the various studied HEAs for payload exploration with a fixed design range in Figs. A1–A3 and range exploration for a fixed payload in Figs. A4–A6.

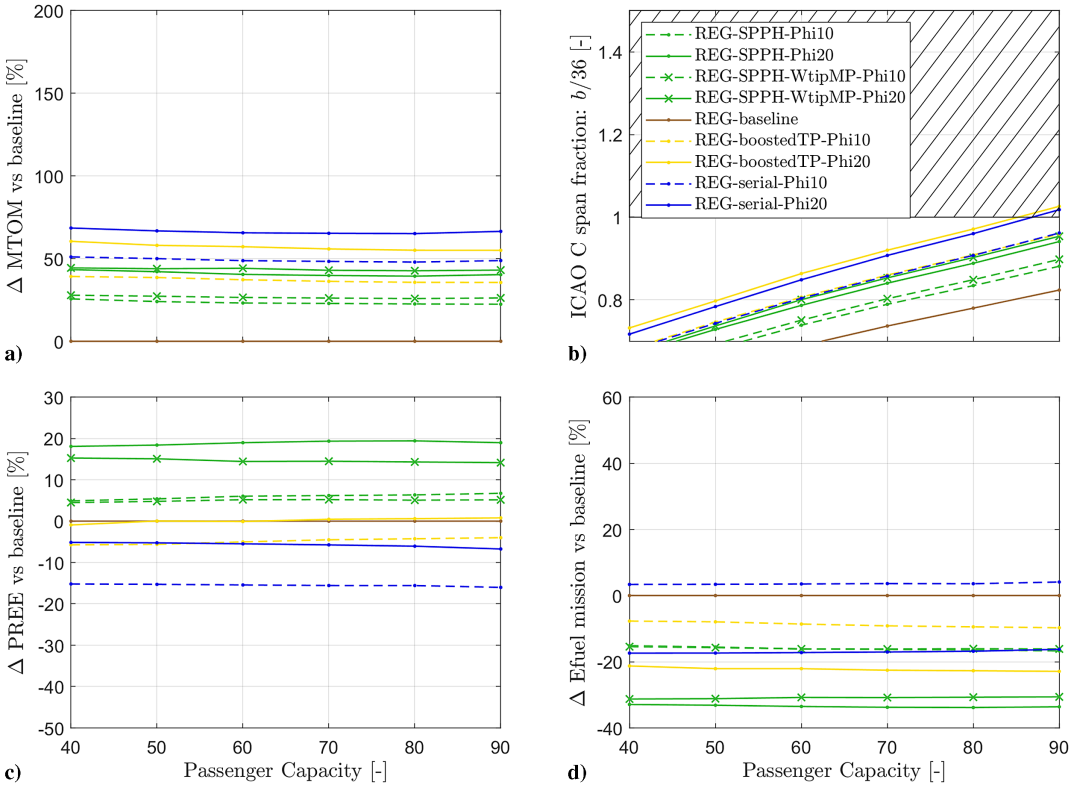

Fig. A1 Payload exploration of regional HEA with 556 km design range.

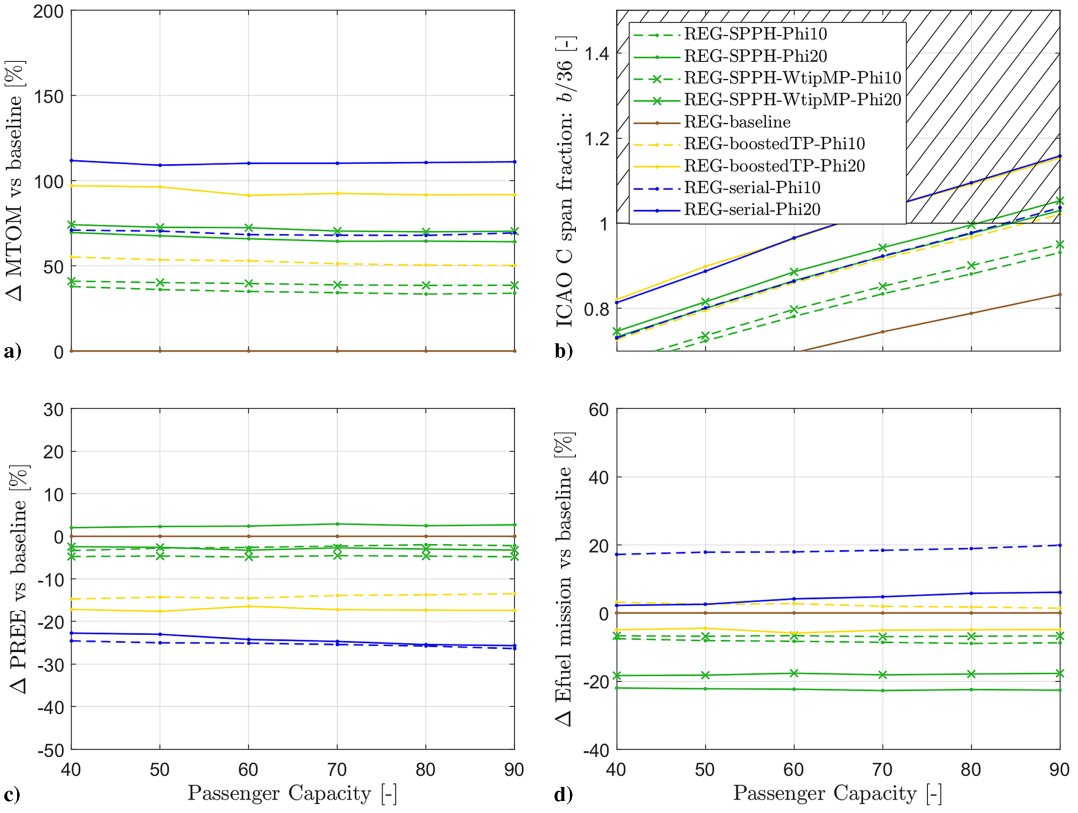

Fig. A2 Payload exploration of regional HEA with 833 km design range.

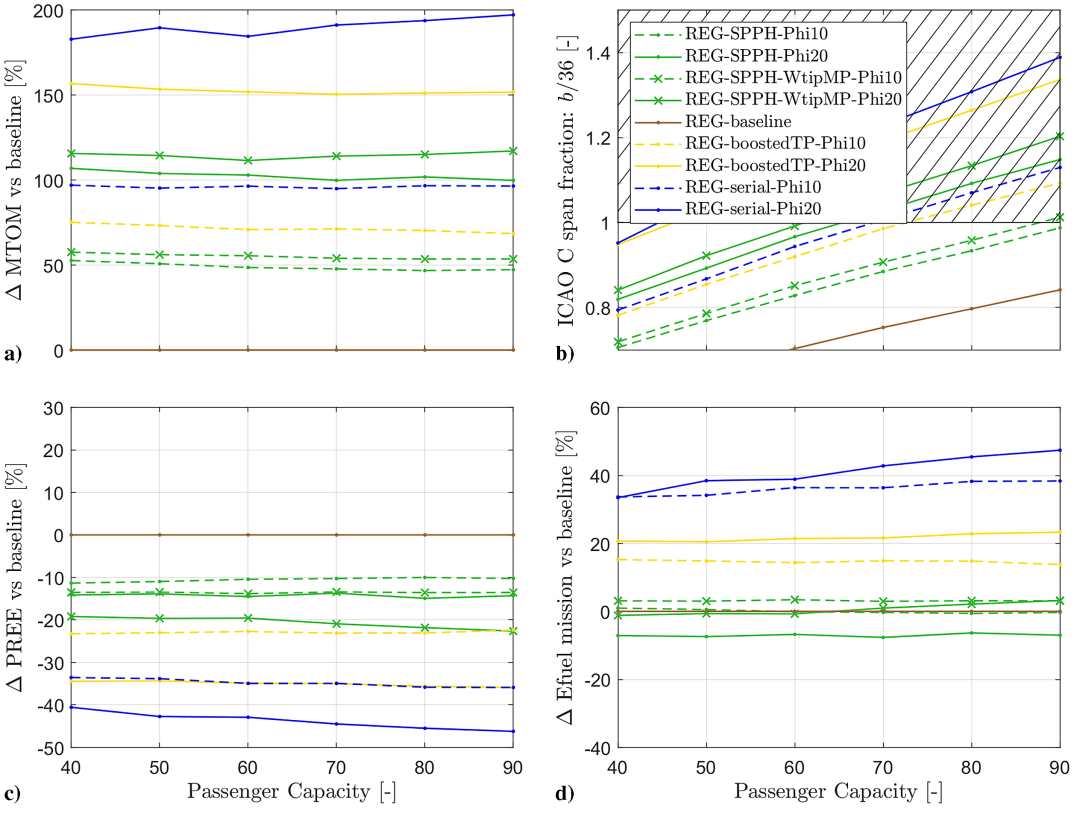

Fig. A3 Payload exploration of regional HEA with 1111 km design range.

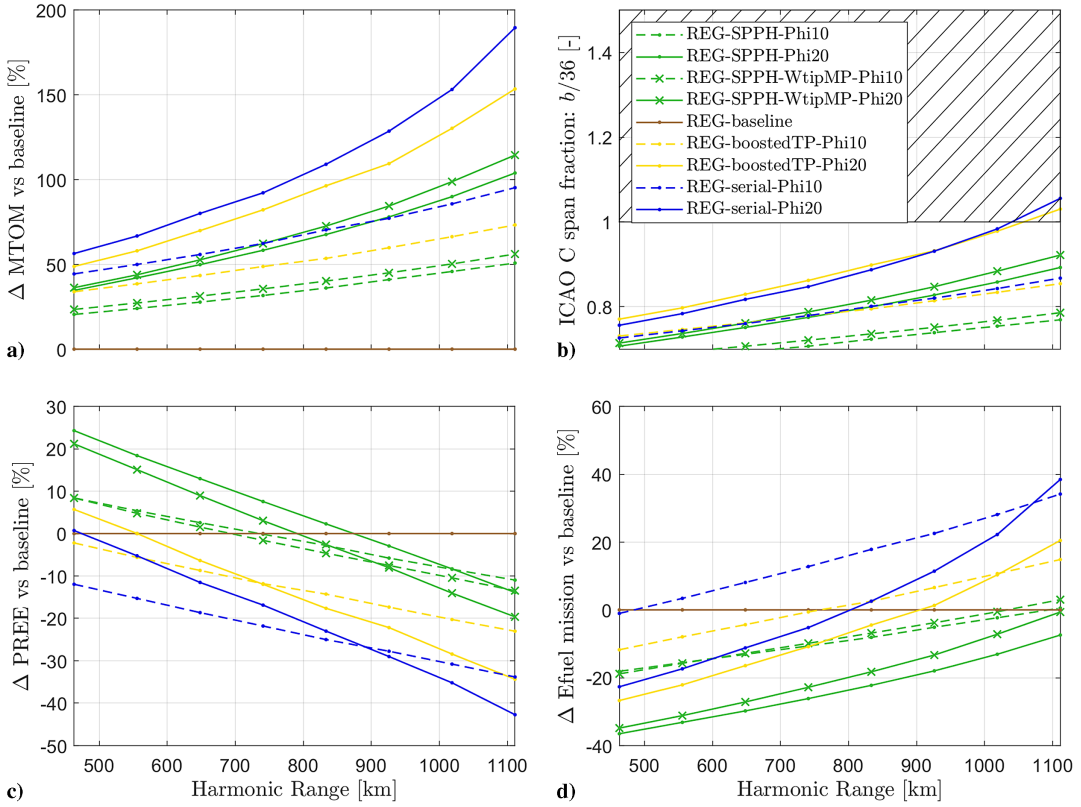

Fig. A4 Range exploration of regional HEA with 50 pax capacity.

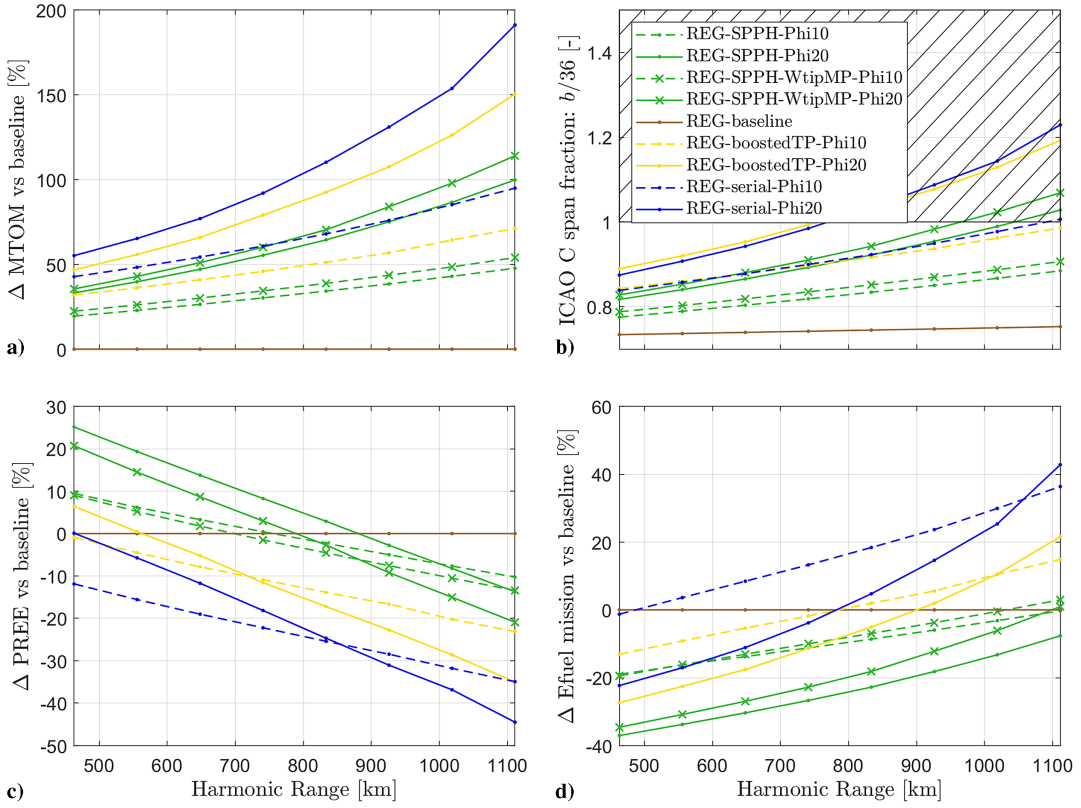

Fig. A5 Range exploration of regional HEA with 70 pax capacity.

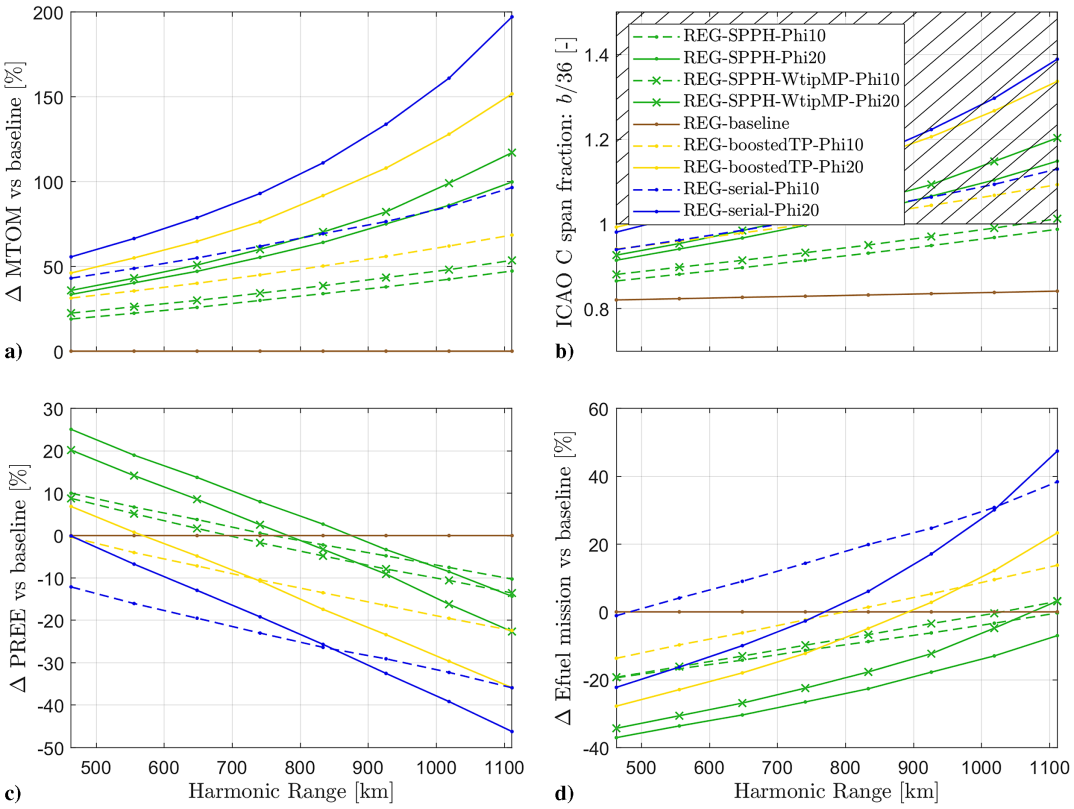

Fig. A6 Range exploration of regional HEA with 90 pax capacity.

Acknowledgments

This research was partially funded by the "CHYLA" project, which received funding from the European Union's Horizon 2020 research and innovation program under Grant Agreement No. 101007715. The authors want to thank Aniello Cozzolino from Piaggio Aerospace for his input regarding the E-STOL.

References

[1] Anonymous, "Flightpath 2050: Europe's Vision for Aviation," Tech. Rept. KI-30-12-812-EN-C, European Commission, Directorate-General for Mobility and Transport, Directorate-General for Research and Innovation, 2011. https://doi.org/10.2777/15458

[2] Felder, J. L., "NASA Electric Propulsion System Studies," NASA TR GRC-E-DAA-TN28410, NASA Glenn Research Center, Nov. 2015, https://ntrs.nasa.gov/citations/20160009274.

[3] Anonymous, *Commercial Aircraft Propulsion and Energy Systems Research: Reducing Global Carbon Emissions*, National Academies Press, Washington, D.C., 2016. https://doi.org/10.17226/23490

[4] Salem, K. A., Palaia, G., and Quarta, A. A., "Review of Hybrid-Electric Aircraft Technologies and Designs: Critical Analysis and Novel Solutions," *Progress in Aerospace Sciences*, Vol. 141, Aug. 2023, Paper 100924. https://doi.org/10.1016/j.paerosci.2023.100924

[5] Tariq, M., Maswood, A. I., Gajanayake, C. J., and Gupta, A. K., "Aircraft Batteries: Current Trend Towards More Electric Aircraft," *IET Electrical Systems in Transportation*, Vol. 7, No. 2, 2017, pp. 93–103. https://doi.org/10.1049/iet-est.2016.0019

[6] Radomsky, L., Keilmann, R., Ferch, D., and Mallwitz, R., "Challenges and Opportunities in Power Electronics Design for All-and Hybrid-Electric Aircraft: A Qualitative Review and Outlook," *CEAS Aeronautical Journal*, Vol. 15, No. 4, 2024, pp. 1–14. https://doi.org/10.1007/s13272-024-00770-6

[7] Sayed, E., Abdalmagid, M., Pietrini, G., Sa'adeh, N.-M., Callegaro, A. D., Goldstein, C., and Emadi, A., "Review of Electric Machines in More-/Hybrid-/Turbo-Electric Aircraft," *IEEE Transactions on Transportation Electrification*, Vol. 7, No. 4, 2021, pp. 2976–3005. https://doi.org/10.1109/TTE.2021.3089605

[8] Brelje, B. J., and Martins, J. R., "Electric, Hybrid, and Turboelectric Fixed-Wing Aircraft: A Review of Concepts, Models, and Design Approaches," *Progress in Aerospace Sciences*, Vol. 104, Jan. 2019, pp. 1–19. https://doi.org/10.1016/j.paerosci.2018.06.004

[9] Cardone, L., Petrone, G., De Rosa, S., Franco, F., and Greco, C., "Review of the Recent Developments About the Hybrid Propelled Aircraft," *Aerotecnica Missili & Spazio*, Vol. 103, No. 1, 2024, pp. 17–37. https://doi.org/10.1007/s42496-023-00173-6

[10] Viswanathan, V., Epstein, A. H., Chiang, Y.-M., Takeuchi, E., Bradley, M., Langford, J., and Winter, M., "The Challenges and Opportunities of Battery-Powered Flight," *Nature*, Vol. 601, No. 7894, 2022, pp. 519–525. https://doi.org/10.1038/s41586-021-04139-1

[11] de Vries, R., Brown, M., and Vos, R., "Preliminary Sizing Method for Hybrid-Electric Distributed-Propulsion Aircraft," *Journal of Aircraft*, Vol. 56, No. 6, 2019, pp. 1–17. https://doi.org/10.2514/1.C035388

[12] Orefice, F., Della Vecchia, P., Ciliberti, D., and Nicolosi, F., "Aircraft Conceptual Design Including Powertrain System Architecture and Distributed Propulsion," *2019 AIAA/IEEE Electric Aircraft Technologies Symposium (EATS)*, AIAA Paper 2019-4465, 2019. https://doi.org/10.2514/6.2019-4465

[13] Finger, D. F., Bil, C., and Braun, C., "Initial Sizing Methodology for Hybrid-Electric General Aviation Aircraft," *Journal of Aircraft*, Vol. 57, No. 2, 2020, pp. 245–255. https://doi.org/10.2514/1.C035428

[14] Cinar, G., Cai, Y., Bendarkar, M. V., Burrell, A. I., Denney, R. K., and Mavris, D. N., "System Analysis and Design Space Exploration of Regional Aircraft with Electrified Powertrains," *Journal of Aircraft*, Vol. 60, No. 2, 2023, pp. 382–409. https://doi.org/10.2514/1.C036919

[15] Pornet, C., Seitz, A., Schmitz, O., Isikveren, A., and Hornung, M., "Methodology for Sizing and Performance Assessment of Hybrid Energy Aircraft," *Journal of Aircraft*, Vol. 52, No. 1, 2014, pp. 341–352. https://doi.org/10.2514/1.C032716

[16] Pornet, C., and Isikveren, A., "Conceptual Design of Hybrid-Electric Transport Aircraft," *Progress in Aerospace Sciences*, Vol. 79, Nov. 2015, pp. 114–135. https://doi.org/10.1016/j.paerosci.2015.09.002

[17] Isikveren, A., Kaiser, S., Pornet, C., and Vratny, P., "Pre-Design Strategies and Sizing Techniques for Dual-Energy Aircraft," *Aircraft Engineering and Aerospace Technology*, Vol. 86, No. 6, 2014, pp. 525–542. https://doi.org/10.1108/AEAT-08-2014-0122

[18] Stückl, S., "Methods for the Design and Evaluation of Future Aircraft Concepts Utilizing Electric Propulsion Systems," Ph.D. Thesis, Technische Universität München, Munich, Germany, 2016, https://nbn-resolving.de/urn/resolver.pl?urn:nbn:de:bvb:91-diss-20160701-1255732-1-0.

[19] Chakraborty, I., and Mavris, D. N., "Integrated Assessment of Aircraft and Novel Subsystem Architectures in Early Design," *Journal of Aircraft*, Vol. 54, No. 4, 2017, pp. 1268–1282. https://doi.org/10.2514/1.C033976

[20] Perullo, C., and Mavris, D., "A Review of Hybrid-Electric Energy Management and Its Inclusion in Vehicle Sizing," *Aircraft Engineering and Aerospace Technology: An International Journal*, Vol. 86, No. 6, 2014, pp. 550–557. https://doi.org/10.1108/AEAT-04-2014-0041

[21] Lee, H., Harris, C. M., Gladin, J. C., and Mavris, D. N., "A Method for Simultaneous Optimization of Power Split and Flight Path Trajectories for Hybrid Electric Aircraft," *AIAA Scitech 2021 Forum*, AIAA Paper 2021-1010, 2021. https://doi.org/10.2514/6.2021-1010

[22] Antcliff, K., Guynn, M., Marien, T., Wells, D., Schneider, S., and Tong, M., "Mission Analysis and Aircraft Sizing of a Hybrid-Electric Regional Aircraft," *54th Aerospace Sciences Meeting*, AIAA Paper 2016-1028, 2016. https://doi.org/10.2514/6.2016-1028

[23] Welstead, J., and Felder, J. L., "Conceptual Design of a Single-Aisle Turboelectric Commercial Transport with Fuselage Boundary Layer Ingestion," *54th AIAA Aerospace Sciences Meeting*, AIAA Paper 2016-1027, 2016. https://doi.org/10.2514/6.2016-1027

[24] Antcliff, K. R., and Capristan, F. M., "Conceptual Design of the Parallel Electric-Gas Architecture with Synergistic Utilization Scheme (PEGASUS) Concept," *18th AIAA/ISSMO Multidisciplinary Analysis and Optimization Conference*, AIAA Paper 2017-4001, 2017. https://doi.org/10.2514/6.2017-4001

[25] Hoogreef, M., de Vries, R., Sinnige, T., and Vos, R., "Synthesis of Aero-Propulsive Interaction Studies Applied to Conceptual Hybrid-Electric Aircraft Design," *AIAA Scitech 2020 Forum*, AIAA Paper 2020-0503, 2020. https://doi.org/10.2514/6.2020-0503

[26] Voskuijl, M., Van Bogaert, J., and Rao, A., "Analysis and Design of Hybrid Electric Regional Turboprop Aircraft," *CEAS Aeronautical Journal*, Vol. 9, No. 1, 2018, pp. 15–25. https://doi.org/10.1007/s13272-017-0272-1

[27] Zamboni, J., Vos, R., Emeneth, M., and Schneegans, A., "A Method for the Conceptual Design of Hybrid Electric Aircraft," *AIAA SciTech 2019 Forum*, AIAA Paper 2019-1587, 2019. https://doi.org/10.2514/6.2019-1587

[28] Orefice, F., Corcione, S., Nicolosi, F., Ciliberti, D., and Rosa, G. D., "Performance Calculation for Hybrid-Electric Aircraft Integrating Aero-Propulsive Interactions," *AIAA Scitech 2021 Forum*, AIAA Paper 2021-1640, 2021. https://doi.org/10.2514/6.2021-1640

[29] Aigner, B., Stumpf, E., Hinz, A., and Doncker, R. W. D., "An Integrated Design Framework for Aircraft with Hybrid Electric Propulsion," *AIAA Scitech 2020 Forum*, AIAA Paper 2020-1501, 2020. https://doi.org/10.2514/6.2020-1501

[30] Sgueglia, A., Schmollgruber, P., Bartoli, N., Benard, E., Morlier, J., Jasa, J., Martins, J. R. R. A., Hwang, J. T., and Gray, J. S., "Multidisciplinary Design Optimization Framework with Coupled Derivative Computation for Hybrid Aircraft," *Journal of Aircraft*, Vol. 57, No. 4, 2020, pp. 715–729. https://doi.org/10.2514/1.C035509

[31] Finger, D. F., Braun, C., and Bil, C., "Comparative Assessment of Parallel-Hybrid-Electric Propulsion Systems for Four Different Aircraft," *Journal of Aircraft*, Vol. 57, No. 5, 2020, pp. 843–853. https://doi.org/10.2514/1.C035897

[32] Graver, B., Rutherford, D., and Zheng, S., "Emissions from Commercial Aviation: 2013, 2018, and 2019," Tech. Rept., International Council on Clean Transportation, Wahington, D.C., 2020, https://theicct.org/publications/co2-emissions-commercial-aviation-2020.

[33] de Vries, R., Hoogreef, M. F. M., and Vos, R., "Aero-Propulsive Efficiency Requirements for Turboelectric Transport Aircraft," *AIAA Scitech 2020 Forum*, AIAA Paper 2020-0502, 2020. https://doi.org/10.2514/6.2020-0502

[34] Quillet, D., Boulanger, V., and Rancourt, D., "Off-Design Performance Analysis of a Parallel Hybrid Electric Regional Turboprop Aircraft," *Journal of Aircraft*, Vol. 60, No. 6, 2023, pp. 1–11. https://doi.org/10.2514/1.C036927

[35] Wroblewski, G. E., and Ansell, P. J., "Mission Analysis and Emissions for Conventional and Hybrid-Electric Commercial Transport Aircraft," *Journal of Aircraft*, Vol. 56, No. 3, 2019, pp. 1200–1213. https://doi.org/10.2514/1.C035070

[36] Palaia, G., and Abu Salem, K., "Mission Performance Analysis of Hybrid-Electric Regional Aircraft," *Aerospace*, Vol. 10, No. 3, 2023, Paper 246. https://doi.org/10.3390/aerospace10030246

[37] de Vries, R., Hoogreef, M. F. M., and Vos, R., "Range Equation for Hybrid-Electric Aircraft with Constant Power Split," *Journal of Aircraft*, Vol. 57, No. 3, 2020, pp. 552–557. https://doi.org/10.2514/1.C035734

[38] Torenbeek, E., *Synthesis of Subsonic Airplane Design*, Springer, Dordrecht, The Netherlands, 1982. https://doi.org/10.1007/978-94-017-3202-4

[39] Roskam, J., *Airplane Design*, DAR Corp., Lawrence, Kansas, 1986.

[40] Obert, E., *Aerodynamic Design of Transport Aircraft*, IOS Press, Amsterdam, The Netherlands, 2009.

[41] Elmendorp, R. J. M., Vos, R., and La Rocca, G., "A Conceptual Design and Analysis Method for Conventional and Unconventional Airplanes," *ICAS 2014: Proceedings of the 29th Congress of the International Council of the Aeronautical Sciences*, International Council of Aeronautical Sciences, Bonn, Germany, Sept. 2014, https://repository.tudelft.nl/islandora/object/uuid%3A1dc55ce5-18c3-4986-b668-f70d9b24aac0.

[42] Onorato, G., Proesmans, P.-J., and Hoogreef, M. F. M., "Assessment of Hydrogen Transport Aircraft- Effects of Fuel Tank Integration," *CEAS Aeronautical Journal*, Vol. 13, No. 4, 2022, pp. 813–845. https://doi.org/10.1007/s13272-022-00601-6

[43] Schut, E. J., and van Tooren, M. J. L., "Design "Feasilization" Using Knowledge-Based Engineering and Optimization Techniques," *Journal of Aircraft*, Vol. 44, No. 6, 2007, pp. 1776–1786. https://doi.org/10.2514/1.24688

[44] Hoogreef, M., and Vos, R., "The Oval Fuselage; A New Structural Design Concept for Blended-Wing-Body Cabins," *Proceedings of RAeS 3rd Aircraft Structural Design Conference*, Royal Aeronautical Soc., United Kingdom, 2012, pp. 1–15.

[45] Vos, R., and Hoogreef, M., "Semi-Analytical Weight Estimation Method for Fuselages with Oval Cross-Section," *54th AIAA/ASME/ASCE/AHS/ASC Structures, Structural Dynamics, and Materials Conference*, AIAA Paper 2013-1719, 2013. https://doi.org/10.2514/6.2013-1719

[46] Schmidt, K., and Vos, R., "A Semi-Analytical Weight Estimation Method for Oval Fuselages in Conventional and Novel Aircraft," *52nd Aerospace Sciences Meeting*, AIAA Paper 2014-0026, 2014. https://doi.org/10.2514/6.2014-0026

[47] Roelofs, M., and Vos, R., "Semi-Analytical Composite Oval Fuselage Weight Estimation," *55th AIAA Aerospace Sciences Meeting*, AIAA Paper 2017-0466, 2017. https://doi.org/10.2514/6.2017-0466

[48] Elmendorp, R. J. M., and La Rocca, G., "Comparative Design & Sensitivity Studies on Box-Wing Airplanes," *Italian Association of Aeronautics and Astronautics—XXV International Congress*, 2019.

[49] de Vries, R., "Hybrid-Electric Aircraft with Over-the-Wing Distributed Propulsion: Aerodynamic Performance and Conceptual Design," Ph.D. Thesis, Delft Univ. of Technology, Delft, The Netherlands, 2022. https://doi.org/10.4233/uuid:ef87dc11-e7b2-4726-a41f-28588d64c58d

[50] Finger, D. F., de Vries, R., Vos, R., Braun, C., and Bil, C., "Cross-Validation of Hybrid-Electric Aircraft Sizing Methods," *Journal of Aircraft*, Vol. 59, No. 4, 2022, pp. 1–19. https://doi.org/10.2514/1.C035428.c1

[51] de Vries, R., Hoogreef, M., and Vos, R., "Preliminary Sizing of a Hybrid-Electric Passenger Aircraft Featuring Over-the-Wing Distributed-Propulsion," *AIAA Scitech 2019 Forum*, AIAA Paper 2019-1811, 2019. https://doi.org/10.2514/6.2019-1811

[52] Raymer, D., *Aircraft Design: A Conceptual Approach*, 6th ed., AIAA, Reston, VA, 2018, p. 479. https://doi.org/10.2514/4.104909

[53] Hoogreef, M., and Bonnin, V., "Scalability Analysis of Radical Technologies to Various Aircraft Class—Part I: Initial Designs," *ICAS 2022 Conference*, 2022, https://www.icas.org/ICAS_ARCHIVE/ICAS2022/data/papers/ICAS2022_0248_paper.pdf.

[54] Romano, D. G., Apuleo, G., and Duda, J., "Affordable and Environmental Friendly Small Commuter Aircraft Improving European Mobility," *International Journal of Aerospace and Mechanical Engineering*,

Vol. 14, No. 9, 2020, pp. 389–397, https://publications.waset.org/pdf/10011410.

[55] Romano, D. G., and Apuleo, G., "Improvement of European Thin Haul Mobility: the Role of Small Green Commuter Aircraft," *IOP Conference Series: Materials Science and Engineering*, Vol. 1226, No. 1, 2022, Paper 012086. https://doi.org/10.1088/1757-899X/1226/1/012086

[56] Cozzolino, A., Apuleo, G., and D'Alesio, P., "Technology Readiness Assessment and Performance Forecast on a 19 Seats E-STOL EIS. 2032," *Journal of Physics: Conference Series*, Vol. 2526, No. 1, 2023, Paper 012016. https://doi.org/10.1088/1742-6596/2526/1/012016

[57] Bonnin, V., Hoogreef, M., and de Vries, R., "Distributed Hybrid-Electric Propulsion Benefits for Span-Limited Aircraft," *AIAA SCITECH 2023 Forum*, AIAA Paper 2023-2098, 2023. https://doi.org/10.2514/6.2023-2098

[58] Wolleswinkel, R., de Vries, R., Hoogreef, M. F. M., and Vos, R., "A New Perspective on Battery-Electric Aviation, Part I: Reassessment of Achievable Range," *AIAA Scitech 2024 Forum*, AIAA Paper 2024-1489, 2024. https://doi.org/10.2514/6.2024-1489

A. Friess
Associate Editor